Title

I. THE RADIATIVE LIFETIME OF THE MERCURY 3P1 STATE. II. THE LIFETIMES AND SELF-QUENCHING COLLISION CROSS-SECTIONS OF FLUORESCENCE FROM VARIOUS v' REGIONS OF THE B3nO+u STATE of I2

Author

Chutjian, Ara.

Publication Date

1966

UNIVERSITY OF CALIFORNIA
Lawrence Radiation Laboratory
Berkeley, California

AEC Contract No. W-7405-eng-48

I. THE RADIATIVE LIFETIME OF THE MERCURY $^3P_1$ STATE

II. THE LIFETIMES AND SELF-QUENCHING COLLISION CROSS-SECTIONS OF FLUORESCENCE FROM VARIOUS v' REGIONS OF THE $B^3\Pi_{0+u}$ STATE OF I_2

Ara Chutjian

January 1966
(Ph. D. Thesis)

DISCLAIMER

I. THE RADIATIVE LIFETIME OF THE MERCURY $^3P_1$ STATE

II. THE LIFETIMES AND SELF-QUENCHING COLLISION CROSS-SECTIONS OF FLUORESCENCE FROM VARIOUS v' REGIONS OF THE $B^3\Pi_{0+u}$ STATE OF I_2

Ara Chutjian

Inorganic Materials Research Division,
Lawrence Radiation Laboratory,
Department of Chemistry,
University of California,
Berkeley, California

January, 1966

ABSTRACT

The lifetime of the mercury 2537Å $^3P_1 - {}^1S_0$ transition is measured in order to check the performance of the lifetime apparatus described here. The measured value is in good agreement with other previous measurements, and the observed increase in lifetime at higher vapor densities is shown to be due to radiation entrapment.

The radiative lifetime of eight vibrational levels from v' = 8 to v' = 100 in the B state of I_2 have been measured, together with I_2-I_2 self-quenching cross-sections for each level. Excitation was made both with atomic lines (5461, 5889-95, 5086Å) and narrow band continua. No significant changes in cross section or lifetime were observed when the peak of the continuum excitation corresponded to the atomic line wavelength. The self-quenching cross sections did not vary with vibrational level, whereas the lifetimes varies by as much as a factor of seven.

The kinetics of the recombination of iodine atoms is discussed, and the resulting formula for the steady-state concentration of atoms using quenching rates measured in the present work is compared with the single piece of experimental datum available.

CONTENTS

I. INTRODUCTION

Certainly one of the more striking aspects of transition probability measurements is the variety of techniques and approaches that have been used. Depending on one's needs, any one of these techniques will, in principle, provide lifetimes of good (<10%) accuracy. Thus, easily vaporizable species can be observed in an equilibrium situation (e.g., sodium atoms sealed in a quartz cell) and their lifetime τ measured by, for instance, the hook method; or perhaps in a non-equilibrium situation in an atomic beam with τ measured by the equivalent width technique, if the rate of vaporization is known. High temperature species (Pd, Co, high temperature molecules like LaO, ScO, YO, ScF) can be observed in a beam using the phase shift method without having to know the particle density; or else by observing the direct decay of radiation after excitation by some resonant wavelength.

In return for his efforts, the researcher obtains f-values - measures of the degree to which an atom undergoing a given transition resembles a classical atom with an elastically bound electron - and Einstein A coefficients of spontaneous emission (for any transition there is the easy conversion between them: $f/A = 1.51\ (g_2/g_1)\ \lambda^2$, where g_2 and g_1 are the statistical degeneracies of the upper and lower states, respectively, and λ the wavelength of the transition). These quantities can then be used to test the validity of a wave function calculation in the case of simpler atoms, and in general allow one to calculate the particle density N where previously only Nf could be obtained. This enables the astrophysicist to translate intensity measurements of certain star absorptions into actual particle concentrations on the star. And it permits the thermodynamicist

to measure equilibrium concentrations of species in the vapor phase, and to obtain equilibrium constants and free-energy functions for the species.

The knowledge of the particle density is a convenient heading under which to group the many methods. The following discussion will thus treat first those methods which do require the particle density N, and then those that are independent of N. For further information, the excellent review article by Foster[1] goes into some of the subtler aspects of the techniques, as well as presenting a broad view of the field.

A. Methods Which Require N

1. Magnetic Rotation

In the ordinary Faraday effect, a beam of plane or circularly polarized light passing through a gas in a magnetic field H will have its plane of polarization rotated by an angle θ.[2] If the gas has an absorption frequency at ω_o, the angle of rotation is

$$\theta(\omega) = \pm \frac{\pi e^3 H \ell}{2m^2c^2} \cdot \frac{zNf}{(\omega-\omega_o)^2}$$

where ℓ is the length of the absorbing column of gas, and z is a number characterized by the splitting factors and intensities of the Zeeman components (ref. 3, p. 133). In order for the above equation to be valid, $(\omega-\omega_o)$ must be large, which means that the absorption takes place in the wings of the incident line where the absorption coefficient is small, so that pressures of the absorbing gas must be kept high, and ℓ be made large.

The frequency ω at which the rotation $\theta(\omega)$ occurs is measured with a spectrograph capable of resolving ω and ω_o, and the final result is a value for Nf, from which the f-value of the line can be gotten if vapor pressure data are known.

If the vapor pressure data are not given, then the variation used by Weingeroff[4,5] can be used to get τ directly. His method measures the difference between the amount of light due to magneto-rotation and background and the amount due to background alone, and the final result is independent of the particle density.

2. Equivalent Width Technique

The measurement of the equivalent width of an absorption line can be used in conjunction with atomic beam techniques to give absolute f-values. The equivalent width is a measure of the total intensity absorbed out of a continuum by a column of gas and has the distinct advantage that it is independent of the spectrograph broadening. It is simply defined as the integrated area in Fig. 1, and is given by

$$W_\lambda = \int_{\text{line}} \frac{I^o - I_\lambda}{I^o} \, d\lambda.$$

The relationship between log W_λ and log Nf is one form of the curve of growth. Knowing the natural and Doppler widths of the simple absorption line, we may calculate log Nf vs log W_λ. We can then plot the measured equivalent width against log N (known through some other procedure), and get f from the shift necessary to superimpose the measured and calculated plots.

In the method of Lawrence, Link, and King[6] the equivalent width of an absorption line of an atom in a beam is combined with a knowledge of the particle density, gotten by measuring the rate of deposit of the atoms on a microbalance, to get f, the defining equation being

$$f = \frac{CQT}{G(B.F.)}$$

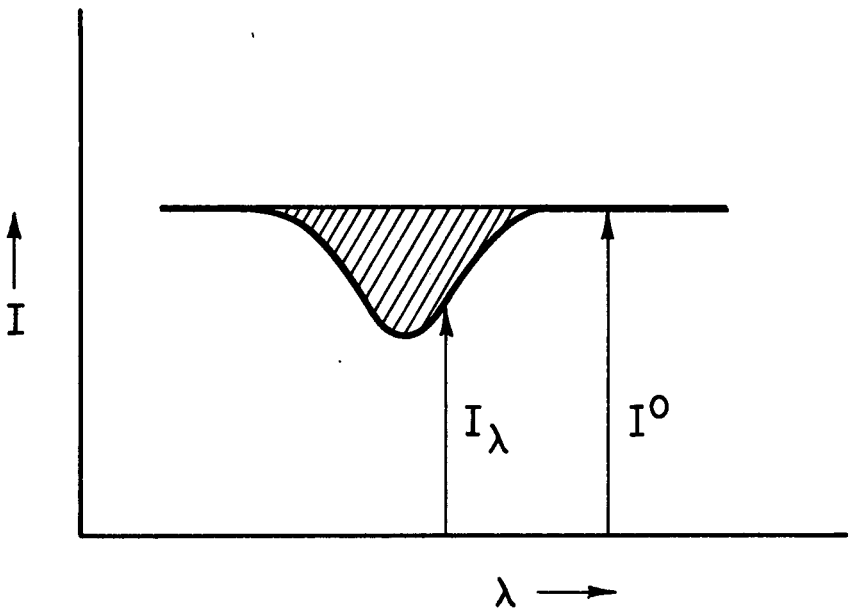

MU-36928

Fig. 1

where C is proportional to Nf from the measured value of the equivalent width, Q is related to the geometry of the beam, T the oven temperature, G the rate of deposit of atoms on the microbalance, and B.F. the Boltzmann factor to compensate for population distribution among possible low-lying states.

3. Anomalous Dispersion (Hook Method).

The measurement of the refractive index of a gas fairly close to an absorption line (where contributions from other lines may be neglected) is the basis of the very popular hook method for measuring relative and absolute f-values. This was first used by Rozhdestvenskii in 1912,[7] and has since been used to accumulate a large body of relative f-values, as well as some absolute measurements.[8,9,10]

Light from a continuous source is passed through two arms of a Jamin-Mach interferometer, one arm containing the vapor under study heated in a furnace, the other being an evacuated compensator tube. The two light beams are combined, and the interference between them analyzed by a spectrograph. A series of hooks appears at the absorption frequency of the sample (see, for example, the hooks obtained by Ostrovskii[11] for the AℓI resonance lines). The quantity Nf is given in terms of the separation of the maxima of the hooks about the absorption line and K, the number of fringes per wavelength interval near the absorption. A knowledge of N is again necessary to get absolute f-values.

B. Methods Which Do Not Require N

1. Coincidence Measurements

A method of lifetime measurement that is not limited to resonance transitions is that of delayed coincidences. Heron, McWhirter and Rhoderick[12] used pulsed 40 eV electrons to excits $3^1P - 2^1S$ and $3^3P - 2^3S$

transitions in helium. The pulse which accelerates the electrons is also used to gate a coincidence counter after a variable time delay. The slope of a log (coincidences) vs pulse delay time gives the lifetime, which was 29 nsec for the 3^1P state at a helium pressure of .005 torr, and 53 nsec at 0.03 torr. The present sensitivity of their apparatus necessitates their working at high pressures where entrapment is taking place. For the nonresonant He $3^3P - 2^3S$ radiation which cannot be absorbed by ground state atoms, they measure a true lifetime of 108 ± 7 nsec.

A different approach used by Branner, et al.[13] which has a potentially wider application is shown in Fig. 2. C_t is the coincidence count of ν_1 and ν_2 photons from the same atom, and C_r that of the photons from different atoms. The lifetime of the intermediate state E_1 can be gotten by delaying the counts C_1 from Channel I before feeding them into the coincidence counter, and using a log C vs delay plot as before to get τ.

2. Direct Decay

The observation of the direct decay of fluorescent radiation over several lifetimes is one of the more straightforward approaches to the problem of lifetime and f-value measurements. The technique here is to use a sufficiently short burst of radiation (light, electrons, x-rays, etc.) or to have a continuous supply of radiation and a fast switch (such as a thyratron, Kerr Cell or Pockel Cell) so that decay of the absorbed radiation can be observed as close in time as possible to the initial excitation.

Bennett[14] has used a thyratron to pulse a hydrogen flash lamp, and one to pulse a photomultiplier after a variable time delay. The lamp had an exponential decay with a lifetime of 1.8 nsec and was pulsed at 5000 cps, and the decay of the fluorescent light integrated by a chart recorder. The fluorescence of acridine in water was observed as a function of tem-

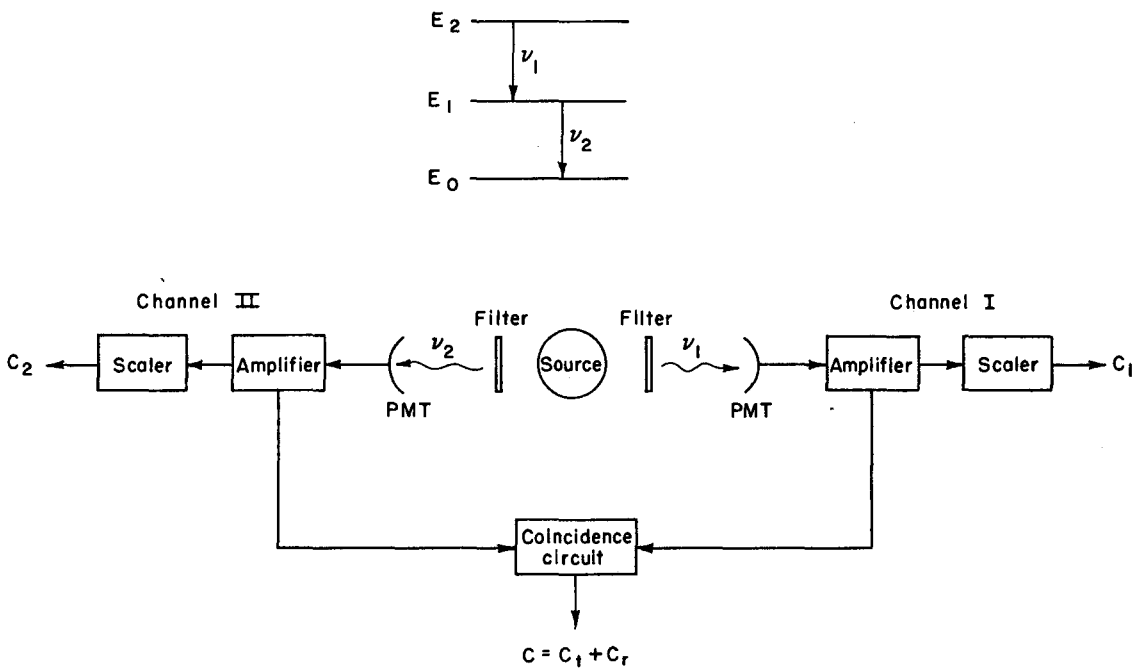
E 2
ν1
E 1
ν2
E 0
Channel III
Filter
Filter
Channel I
C2
Scaler
Amplifier
ν2
Source
ν1
Amplifier
Scaler
C1
PMT
PMT
Coincidence circuit
C = C1 + Cr
MU-36929

Fig. 2

perature, and lifetimes as short as 2.3 nsec were measured.

Steingraber and Berlman[15] have used a similar apparatus with a Type N pulse sampling unit in a Tektronix 531 Oscilloscope for display of the fluorescence. They actually fit their observed intensity vs time curves with the convolution of the impulse response function of the system (its response to the hydrogen flash lamp alone) and the decay function $e^{-t/\tau}$ of the sample, with τ as the free variable.

3. Optical Double Resonance

This technique could also be called the study of the depolarization of the resonance radiation by radio-frequency magnetic fields. A detailed analysis and description of the first results obtained are given by Brossel and Bitter[16] in studying the fluorescence from the $^3P_1$ sublevels of mercury. Mercury atoms are placed in a magnetic field of a few hundred gauss and π-polarized resonance radiation used to excite the atoms to the $m = 0$ Zeeman sublevel of the $^3P_1$ state. A rotating magnetic field induces $m = 0 \rightarrow m = \pm 1$ transitions, and the resultant decrease in $\pi(\Delta m = 0)$ over $\sigma(\Delta m = \pm 1)$ fluorescence intensity is noted. A plot of this difference against the magnetic field strength gives bell-shaped curves whose half-widths are related to the lifetime of the upper state.

Improvements in this technique by Lurio and Novick[17] and by Byron, McDermott and Novick[18] have allowed them to make observations on the $^1P_1$ state of cadmium at much lower vapor densities where entrapment and collision broadening are negligible.

4. Level Crossing

Recently, the method of intersecting energy levels has been applied by Colegrove, Franken, Lewis and Sands[19] and Franken[20] to the measurement of the ^3P multiplet separations in helium. Kibble and Series[21] and Rose and Carovillano[22] give a lucid description of the process.

The basis of the method is to observe the change in the resonance radiation intensity in fluorescence or transmission in the case where two excited Zeeman sublevels in the upper state intersect. If we label the two sublevels a and b, then in the field-free case they will be split by an amount Δ_o which will be larger than the average width $\bar{\gamma} = \frac{1}{2}(\gamma_a + \gamma_b)$ of the states. However, if the separation is made zero by an external magnetic field, and if the incident radiation is broad enough to excite a and b, then there will be a contribution to the fluorescence radiation due to interference between the two levels. The change is angle dependent and is observed in some fixed direction; the total intensity of fluorescence remains the same in the crossed and field-free cases.

The procedure is to observe the sharp resonance in the fluorescence intensity as the field is varied through the cross-over value. The width at half-maximum is just 2γ, from which the lifetime of the upper state is obtained (usually, γ_a and γ_b can be taken as equal). Thus, the $^3P_2$ and $^3P_1$ levels of helium are split by 2291 Mc/s in the absence of a magnetic field, but the $J = 1$, $m = 0$ and $J = 2$, $m = 2$ states can be "tuned" to cross at a field of approximately 600 gauss, whereupon an increase in the fluorescence intensity is seen.

Thaddeus and Novick[23] observed the crossover of $F = \frac{1}{2}$, $m_F = -\frac{1}{2}$ and $F = \frac{3}{2}$, $m_F = \frac{3}{2}$ states in Cd^{111} and Cd^{113} at 2055 and 1964 gauss respectively. The bandwidths of the resonances (as displayed on a scope) gave about twice the expected lifetime of the $^3P_1$ state, which they presume to arise from field inhomogeneities across their sample.

5. Phase Shift

Here, the phase shift between a beam of exciting radiation and fluorescent light of the same or different wavelength is measured, the shift being due to the finite lifetime of the excited atom or molecule.

A complete description of the important relations is given by Berg,[30] and another more compact derivation for the fluorescence intensity and the phase shift is given by Foster[1] in which the fluorescence intensity $I_f(t)$ is represented by the convolution of the exciting intensity $I_o(t)$ and the decay function $\phi(t) = e^{-t/\tau}$

$$I_f(t) = C \int_o^\infty I_o(t-t')\, e^{-t'/\tau}\, dt'$$

where C is a constant containing Nf, the scattering geometry, and widths of the exciting and absorbing lines.

If we let $I_o(t) = A + B \cos \omega t$, then

$$I_f(t) = C \int_o^\infty [A + B \cos \omega(t-t')]\ e^{-t'/\tau}\ dt'$$

$$= \tau C \left[A + \frac{B}{(1+\omega^2\tau^2)^{1/2}} \cos(\omega t - \theta)\right] \qquad (1)$$

where the phase shift θ is

$$\tan \theta = \omega\tau. \qquad (2)$$

The constants A, B, and C have to do with the absolute intensity of fluorescence which is not usually of interest. From Eq. (1) we see that the amplitude of the modulation has been reduced from B to $B/(1 + \omega^2\tau^2)^{1/2}$, and one could obtain τ by measuring the difference in the percent modulation in the incident and fluoresced light. This is usually not as accurate, however, as measuring θ directly in Eq. (2). Equation (2) also shows that θ is always less than $\pi/2$ in order that the lifetime be finite. The frequency ω should be chosen for the apparatus so that $\omega\tau \sim 1$ in order to have conveniently large phase shifts.

Demtröder[25] and Hulpke, Paul and Paul[26] have used the phase shift technique with a supersonic grating modulator to measure ten atomic lifetimes from 1.59 X 10^{-8}(Na) to 3.29 X 10^{-7} sec (Mg). Lawrence[27] has used electron excitation to measure lifetimes and f-values in CO^{+}. His electron source can be modulated at nine fixed frequencies spaced logarithmically from 0.54 Mc to 54 Mc so that any cascading contributions to the emission can be detected.

II. DESCRIPTION OF THE ELECTRONICS

A block diagram of the long lifetime half of the lifetime apparatus previously used by Berg and Rosenblatt is shown in R. Berg's thesis (ref. 30, p.24). Before any extensive lifetime measurements were made, it was decided that the versatility of the instrument for future applications would be increased if there were a convenient way of changing the modulation frequency so that $\omega\tau$ could always be made close to unity for a comfortably large 45° phase shift. In the older arrangement, the motor speed control (MSC) signal to the wheel was taken before the 60 kc to 1 kc heterodyne stage so that any higher modulation frequency would require two heterodyne stages: one from the higher frequency to 60 kc where a part of the signal would be fed back to the MSC amplifiers; and from 60 kc to 1 kc where all the phase measurements would be made.

The revision involved taking the feedback to the MSC at 1 kc, thus eliminating the 60 kc heterodyne stage along with a troublesome automatic frequency control (AFC) unit which required frequent adjustment. Only one beat-down stage is required for each frequency chosen, and it is necessary to construct only a beat-frequency oscillator (BFO) and two mixer channels for that frequency. At present, there is a BFO and mixer for 100 kc and 360 kc. The wheel then modulates at 99 kc and 359 kc respectively, and the difference frequency of 1 kc is fed to the amplifiers and phase shifters of each channel. A block diagram of the apparatus is shown in Fig. 3.

A. Heterodyne Circuit

The heterodyne circuits for 100 kc and 360 kc are identical. Minor differences arise from the LC of the tuned plate circuits and from different amounts of feedback to the oscillator crystal in each case.

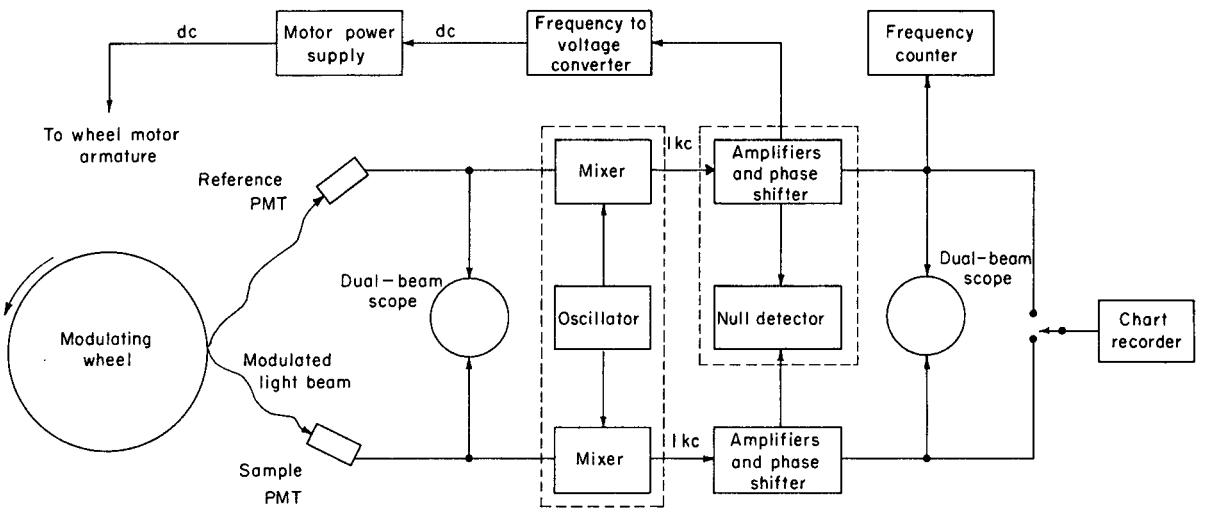
dc
Motor power supply
dc
Frequency to voltage converter
Frequency counter
To wheel motor armature
Reference PMT
Mixer
1 kc
Amplifiers and phase shifter
Dual-beam scope
Modulating wheel
Oscillator
Null detector
Dual-beam scope
Chart recorder
Modulated light beam
Mixer
1 kc
Amplifiers and phase shifter
Sample PMT
MU-36893

Fig. 3

The oscillator is a modified Pierce crystal-controlled circuit, with the feedback controlled by C_8 and R_{13} (see Figs. 4 and 5). The grid-leak bias on the 6AK5 tube should have a time constant of the crystal period; e.g., for 100 kc, $\tau_{osc} = 10^{-5}$ sec, and $R_{10}C_7 = (39X10^{-12})(0.47X10^{6}) = 1.8X10^{-5}$ sec.

The two cathode followers V_2 and V_4 prevent loading of the oscillator, and also prevent any coupling between the two channels through the oscillator. The signal at pin 2 of the 6BA7 mixer tube is 15 v p-p, and the grid-cathode voltage is -7 v. The signal amplitude on this pin is governed by the capacitors C_9 and C_{10} (referred to the 100 kc BFO) in the voltage divider chain on the plate of the 6AK5 tube.

The voltage gain of the four input Miller transformers in both circuits varies from 20 to 30.

B. Frequency to Voltage Converter

The heart of this frequency control circuit in Fig. 6 is the 6BN6 phase discriminator tube.[28] A portion of the 1 kc reference signal is divided into two parts, one shifted approximately 90° in phase with respect to the other, and the signals clipped to a 16 v p-p value and fed onto the limiter (pin 2) and quadrature (pin 6) grids of the 6NB6 tube.

This tube operates between cut-off and saturation, and will begin to conduct when the limiter and quadrature grids are both ≈ - 1 v., with the plate current quickly reaching saturation upon further increase in either voltage. During operation, the limiter grid swings 10.8 v. about a -3.5 v self-bias, and the quadrature grid 13.2 v about a -2.5 v self-bias.

The length of time the tube is "on" (conducting) depends on the phase relation between the two grids which is determined by the frequency deviation from 1 kc of the incoming signal. An increase in the frequency

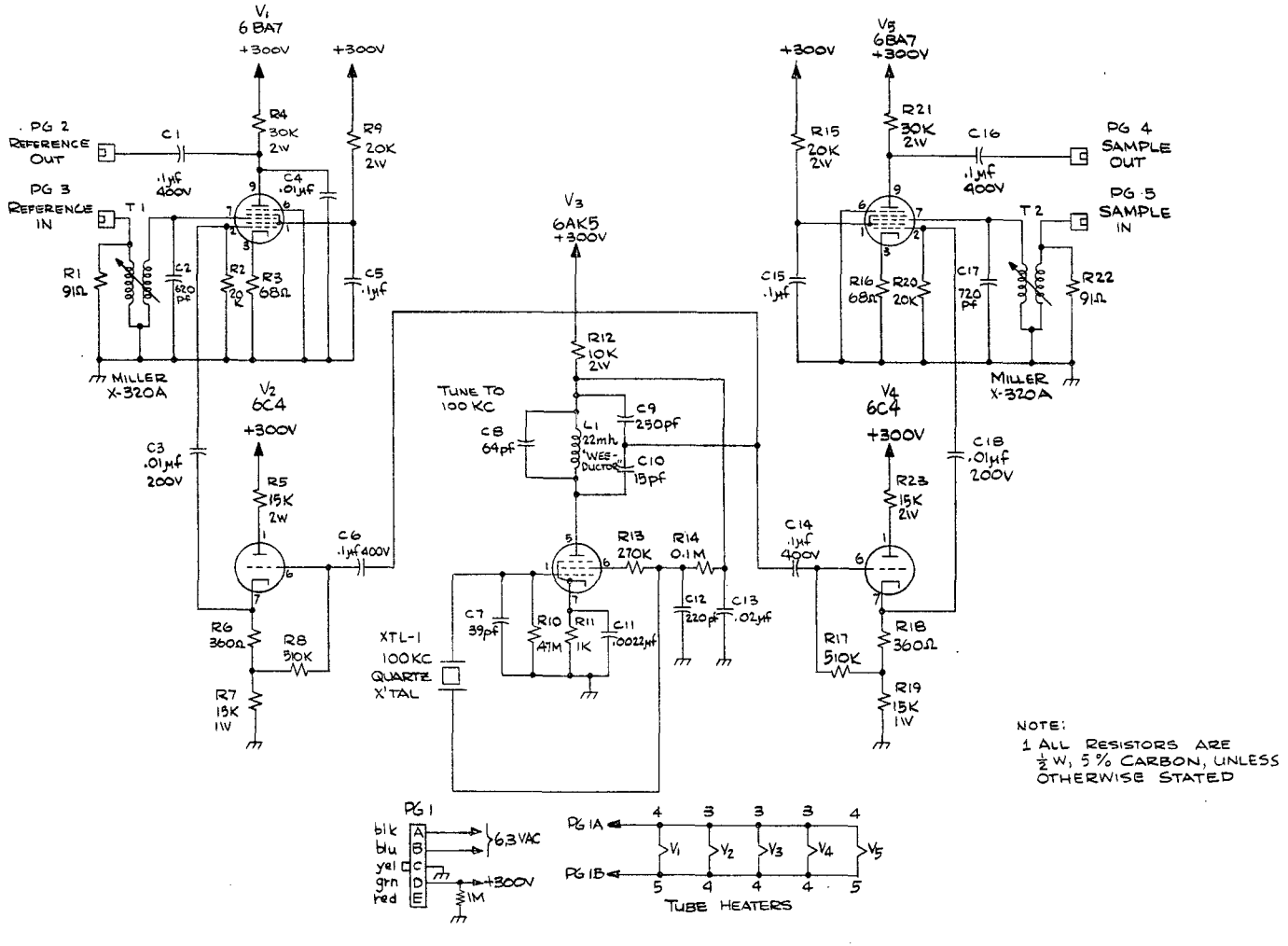

MUB-8627

Fig. 4

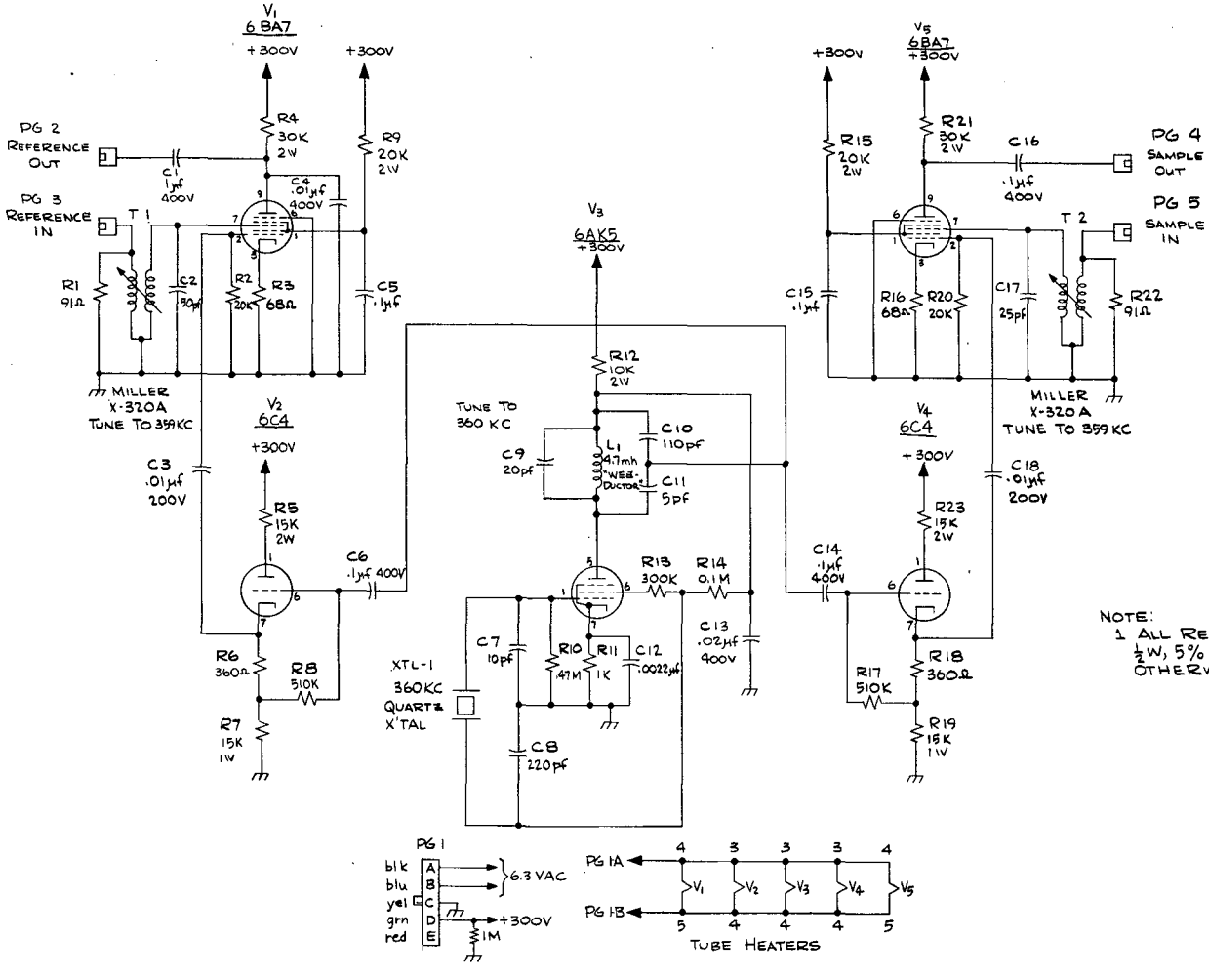
V1
6BA7
+300V
+300V
R4
30K
2W
R9
20K
2W
PG 2
REFERENCE
OUT
C1
.1μf
400V
C4
.01μf
400V
PG 3
REFERENCE
IN
T1
R1
91Ω
C2
50pf
R2
20K
R3
68Ω
C5
.1μf
MILLER
X-320A
TUNE TO 359KC
V2
6C4
+300V
C3
.01μf
200V
R5
15K
2W
C6
.1μf 400V
R6
360Ω
R8
510K
R7
15K
1W
V3
6AK5
+300V
R12
10K
2W
TUNE TO
360 KC
C9
20pf
L1
4.7mh
"WEE-DUCTOR"
C10
110pf
C11
5pf
R13
300K
R14
0.1M
C13
.02μf
400V
C7
10pf
R10
.47M
R11
1K
C12
.0022μf
XTL-1
360KC
QUARTZ
X'TAL
C8
220pf
V5
6BA7
+300V
+300V
R15
20K
2W
R21
30K
2W
C16
.1μf
400V
PG 4
SAMPLE
OUT
PG 5
SAMPLE
IN
T2
C15
.1μf
R16
68Ω
R20
20K
C17
25pf
R22
91Ω
MILLER
X-320A
TUNE TO 359KC
V4
6C4
+300V
C18
.01μf
200V
R23
15K
2W
C14
.1μf
400V
R17
510K
R18
360Ω
R19
15K
1W
PG 1
blk
blu
yel
grn
red
A
B
C
D
E
6.3 VAC
+300V
1M
PG 1A
PG 1B
V1
V2
V3
V4
V5
TUBE HEATERS
NOTE:
1 ALL RESISTORS ARE
½W, 5% CARBON, UNLESS
OTHERWISE STATED.
MUB-8626

Fig. 5

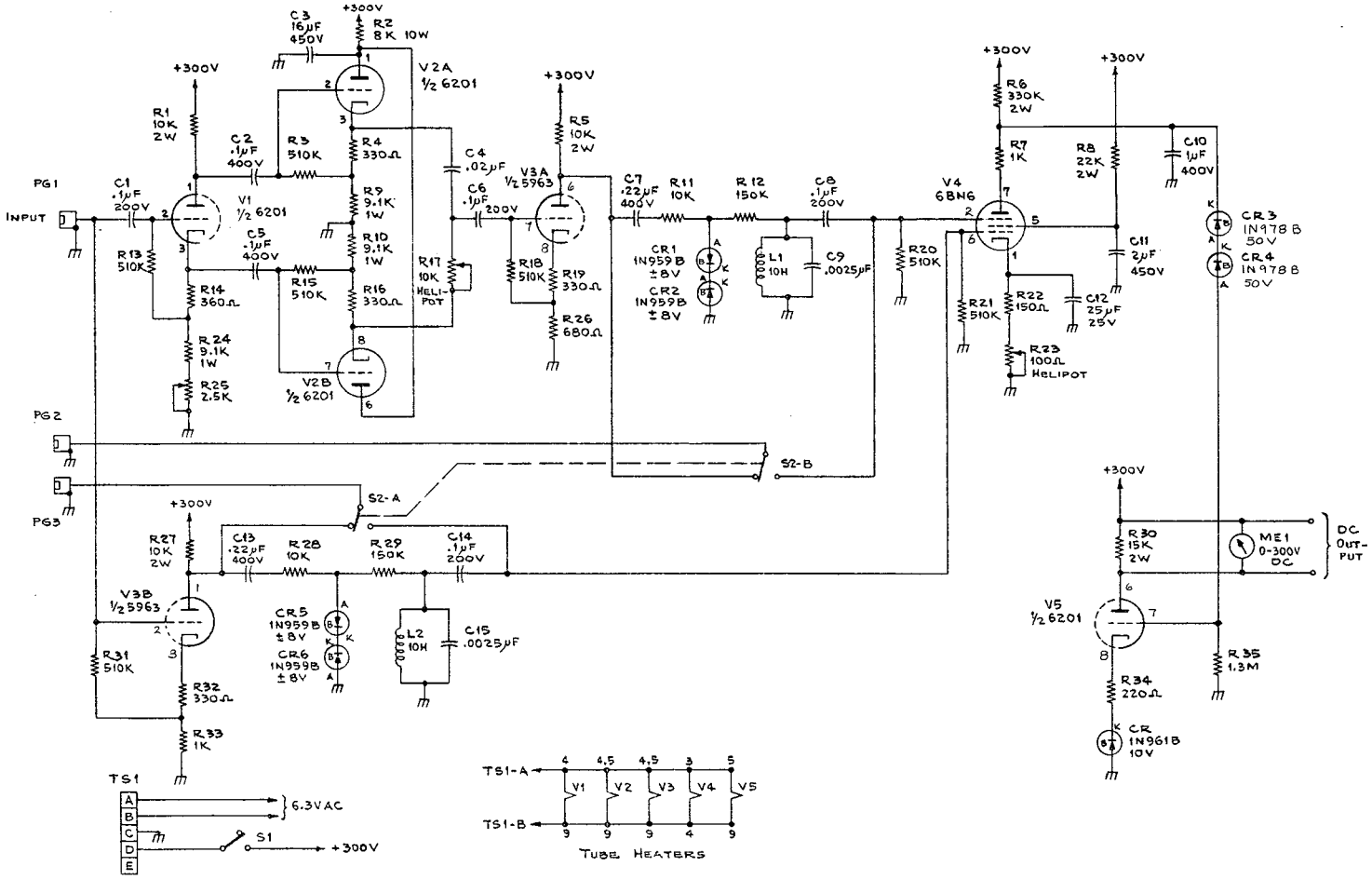

MUB-8623

Fig. 6

(wheel slowing down) will decrease the time the tube is on (relative to the center frequency point) by advancing the phase between the limiter and quadrature grids. This causes a dip in the plate output voltage, an increase in the grid-cathode potential of the subsequent beam power tubes in the motor speed-control power supply, and therefore an increase in the DC current supplied to the motor armature, thus speeding the wheel up. The opposite holds true for a decrease in the reference frequency (wheel speeding up). The maximum current will flow when the phase between the two grids is 0°, causing the tube to conduct on the positive half of both signals.

The plate output voltage as measured by the meter across the plate resistor is plotted against $f_{osc} - f_{wheel}$ in Fig. 7. The tail and the peak of the plot correspond to the tube "off" and "on" state, respectively.

To measure the gain of the circuit, defined as Δ(output voltage)/Δ(input frequency), a standard 1 kc signal from a signal generator is fed into the reference channel phase shifter, and the amplitude fixed at 15 v. p-p on the 1 kc scope. The meter output reading is set at "60" by adjusting the phases on the two grids via R_{17}. The signal frequency is then changed in 10 cps intervals from 900 to 1100 cps, and the meter reading recorded. A typical curve will have a linear negative slope of from 0.85 to 1.05 volts/cycle.

There is a region from 1820 to 1910 cps where the wheel also tends to lock in. However, the gain here is only ~ 0.5 v/cycle, and by proper adjustment of the Variac controls on the motor power supply, the wheel can be made to "run out" of this well, and lock-in in the higher gain region.

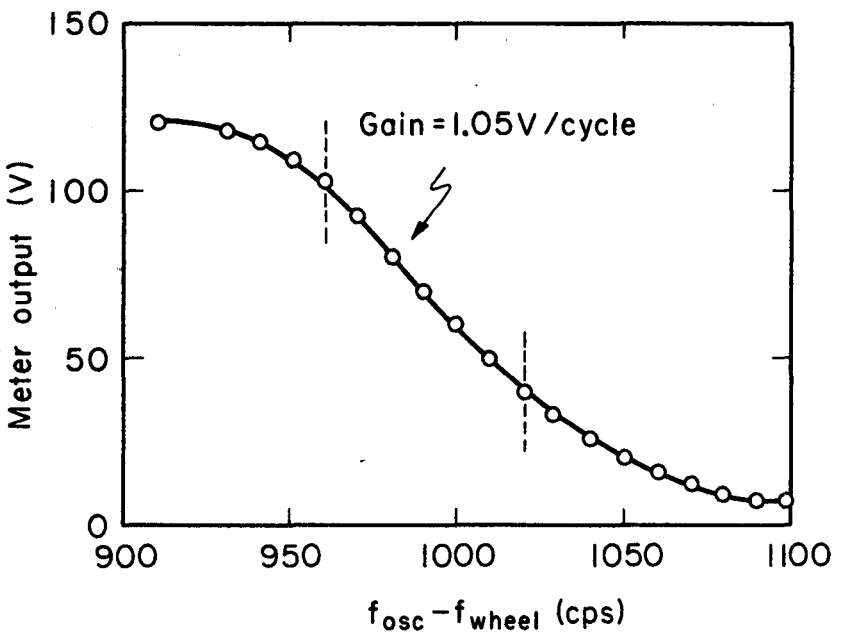

MU-36896

Fig. 7

Another possible lock-in region is on the positive slope of $f_{wheel} - f_{osc}$ [= - $(f_{osc} - f_{wheel})$]. The wheel would then modulate at 361 kc, and the difference 361 - 360 = 1 kc taken.

As for the other circuit components, the actual phase shifting is done by $R_{17}C_4$, where $\tan \phi/2 = \omega R_{17}C_4$. The arrangement of the two cathode followers V2A and V2B fed by the phase inverter V1 insures that the amplitude on pin 7 of V3A remains constant as the phase is shifted (ref. 29, p. 109). The outputs of V3A and V3B are clipped to 16 v p-p and filtered via an LC circuit tuned to 1 kc. This reduces the sensitivity of the output voltage to amplitude variations (caused by scratches on the wheel, lamp intensity fluctuations) by picking out only the 1 kc Fourier harmonic of the clipped signal. The actual change in the beat frequency with feedback amplitude is shown in Fig. 8. Thus, for a change from 56 to 86 volts unclipped limiter grid signal, the beat frequency changes by 2 cps. With the stable light sources used, the variation on the limiter grid was never more than 2 v.

C. Phase Detector

The analysis of the phase detector given by Jerry Sakai (ref. 29, p.118) in incorrect. The output meter is sensitive to the difference in DC levels between points C and D which arises after the rectification of the signals at A and B. Sakai's treatment first subtracts the voltages e_A and e_B, then rectifies the difference. This gives, after correcting his Eqs. (12a) and (12b), the result $e_A - e_B = 2 \sin \omega t$, which contains no phase information at all!

Following his equivalent circuit shown in an identical form in Fig. 9, we see that the voltage at A is the sum of $e_A = \sin \omega t$ and $e_2 = \sin (\omega t + \xi)$;

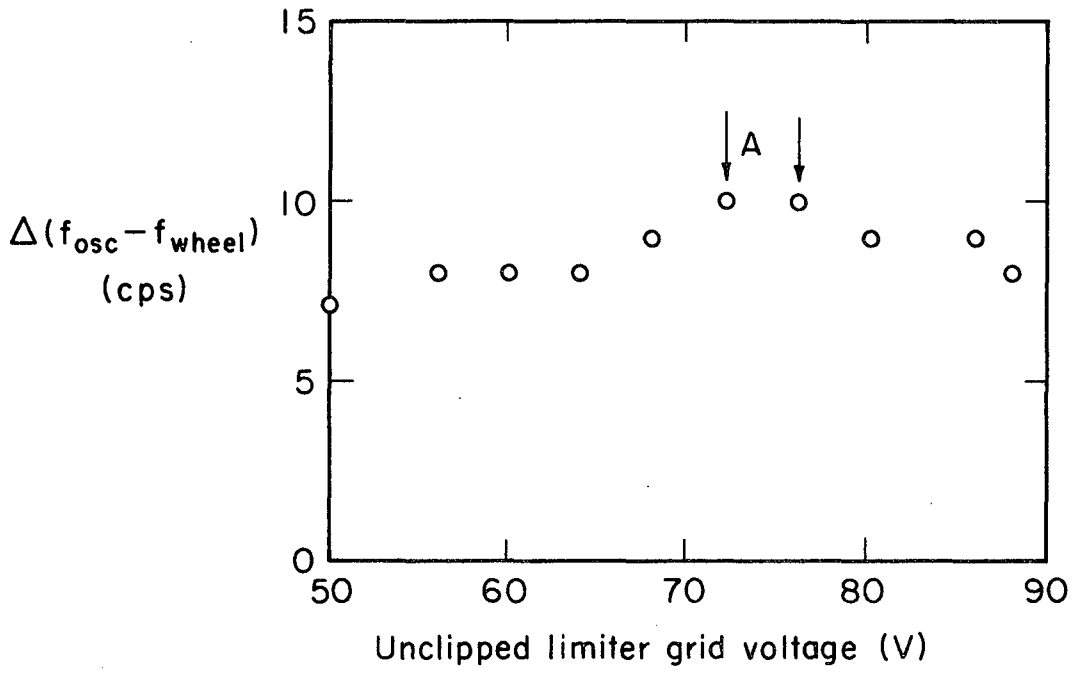
15
10
5
0
A
$\Delta(f_{osc} - f_{wheel})$
(cps)
50
60
70
80
90
Unclipped limiter grid voltage (V)
MU-36898

Fig. 8

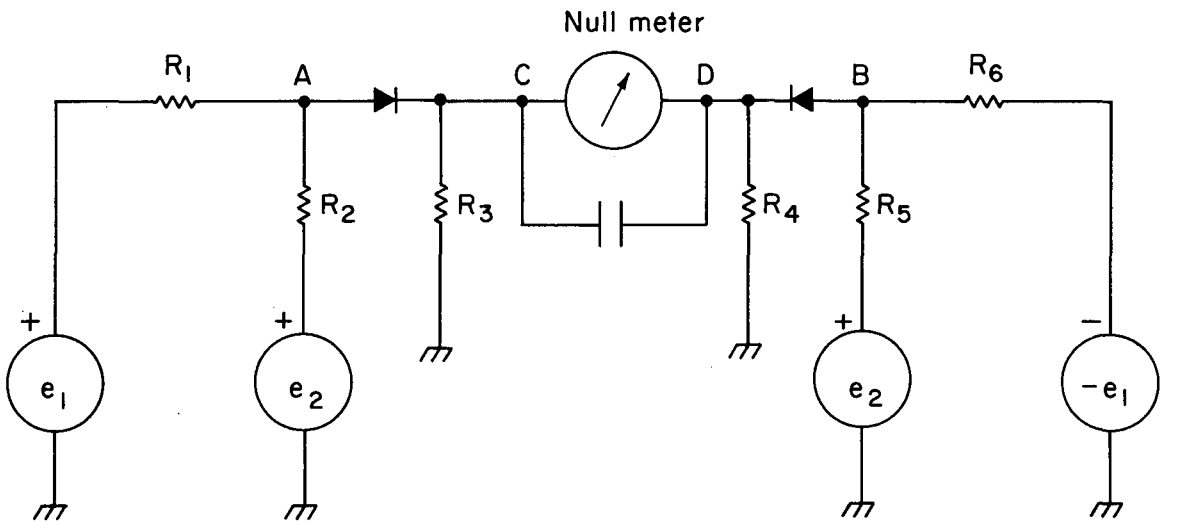

Fig. 9

and the voltage at B is $-e_1 = -\sin \omega t$ and $e_2 = \sin (\omega t + \xi)$. These sums may be written as

$$e_A = e_1 + e_2 = 2 \cos \xi/2 \sin (\omega t + \xi/2)$$

$$e_B = e_1 + e_2 = 2 \sin \xi/2 \cos (\omega t + \xi/2)$$

so that e_A and e_B are 90° out of phase. However, since it is the rectified DC level which deflects the phase meter, it is necessary to find the DC level of the positive cycle of each signal averaged over its respective full cycle. This is just the constant term $\frac{a_o}{2}$ in the Fourier analysis of the half-waves, where the function is

$$e = e_A \quad -\frac{\xi}{2} < \omega t < -\frac{\xi}{2} + \pi$$

$$= 0 \quad -\frac{\xi}{2} + \pi < \omega t < -\frac{\xi}{2} + 2\pi$$

and

$$e = e_B \quad -\frac{\xi}{2} - \frac{\pi}{2} < \omega t < -\frac{\xi}{2} + \frac{\pi}{2}$$

$$= 0 \quad -\frac{\xi}{2} + \frac{\pi}{2} < \omega t < -\frac{\xi}{2} + \frac{3\pi}{2}$$

Letting a_o^A be the DC level of e_A at point C after rectification, a_o^B that at D, we have

$$a_o^A = \frac{2 \cos \xi/2}{\pi} \int_{-\xi/2}^{-\xi/2+\pi} \sin (\omega t + \xi/2) \, d(\omega t) = \frac{4 \cos \xi/2}{\pi}.$$

$$a_o^B = \frac{2 \sin \xi/2}{\pi} \int_{-\xi/2-\pi/2}^{-\xi/2+\pi/2} \cos (\omega t + \xi/2) \, d(\omega t) = \frac{4 \sin \xi/2}{\pi}.$$

The meter then sees $a_o^A - a_o^B = \frac{4}{\pi} (\cos \xi/2 - \sin \xi/2)$, which is zero at $\xi = \pm 90°$. This confirms the result previously cited; i.e., the phase detector shows a null when the reference and sample signals are 90° out of phase.

From the analysis, we must have $-e_1$ and e_1 of equal magnitude, and

the adjustment can be made by means of the "Balance 2" resistor on the output of the phase inverter. However, it was found that although the meter could be balanced in this way, the signals e_1 and $-e_1$ were not identical in form. The two waveforms were made identical with the addition of a cathode follower stage after the plate and cathode of the phase inverter. These stages balanced the impedance looking back from the two rectifier diodes.

The analysis given above shows that the meter deflection should be zero when the reference or sample signal is zero, which agrees with observation. Also, the amplitudes of e_1 and e_2 do not necessarily have to be equal, and small differences (0.5v in 12) in the amplitude of the unclipped signals were tolerated.

1. Balance Adjustments

On the cathode of each phase inverter in the reference and sample channels there is a "Balance" potentiometer which insures that the signals from the plate and cathode are equal in magnitude. Each inverter drives its respective RC phase shifter, and the adjustment is made so as to minimize the AC signal at point A in Fig. 10 (and at equivalent position in Fig. 11). The balanced signal is ~ 100 - 300 mv. in size.

The phase detector meter, however, is not as sensitive to these adjustments as it is to that of the third inverter which drives the detector. This adjustment is made with a 15v p-p reference signal - with no sample signal present - by turning the "Balance 2" potentiometer until the meter is zeroed. This can also be done by looking back into the detector with the oscilloscope connected to the "ϕ Detector Input" plug, and minimizing the AC seen on the scope.

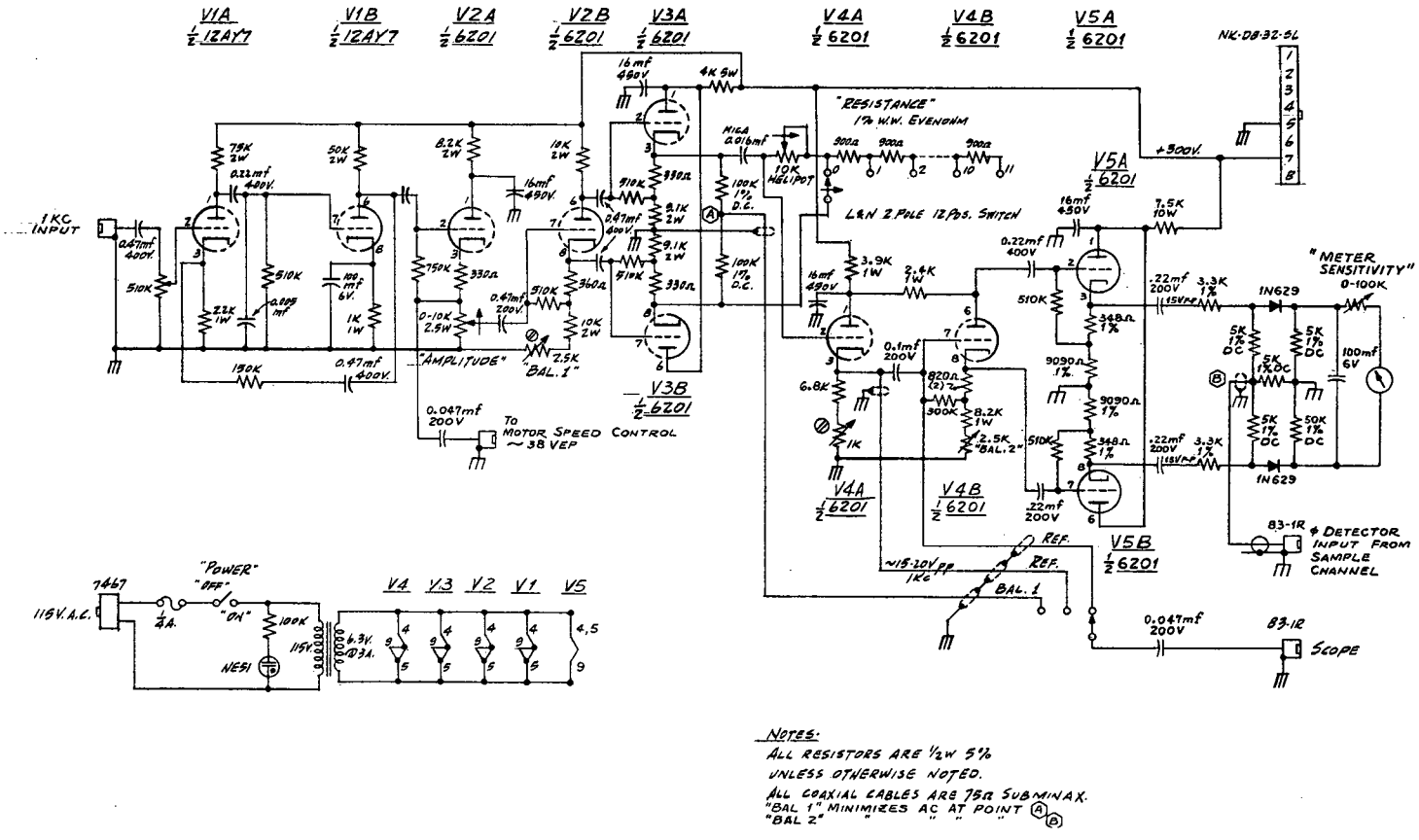

NOTES:
ALL RESISTORS ARE ½W 5%
UNLESS OTHERWISE NOTED.
ALL COAXIAL CABLES ARE 75Ω SUBMINAX.
"BAL 1" MINIMIZES AC AT POINT (A)(B)
"BAL 2" " " " " "

MUB-8624

Fig. 10

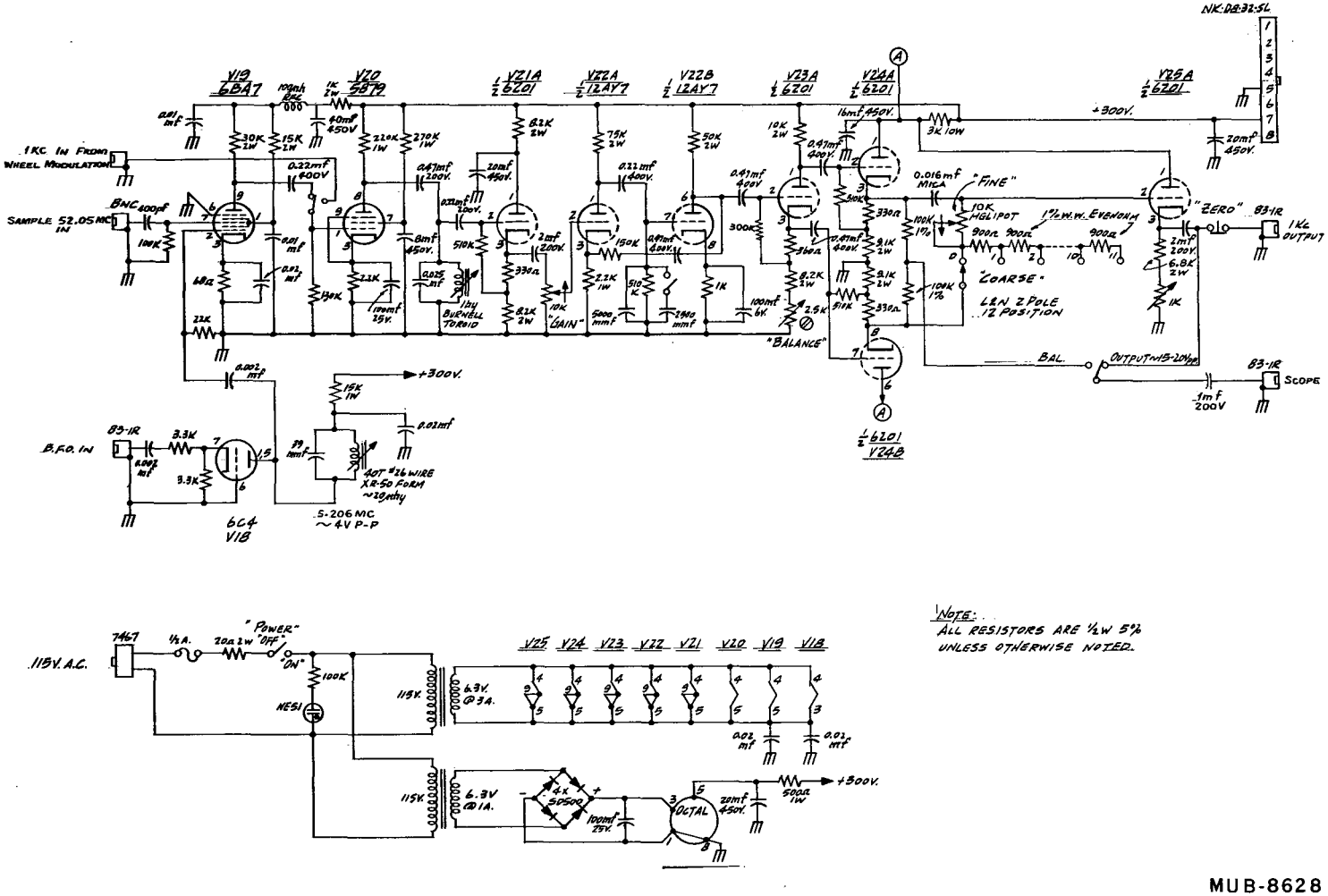

NOTE:
ALL RESISTORS ARE ½W 5% UNLESS OTHERWISE NOTED.

MUB-8628

Fig. 11

The same size sample signal - with no reference signal - should also balance the meter if the signal divides evenly across the two 5k 1% resistors in the detector. However, the meter can detect a 0.1% imbalance of signal, and since the precision resistors are only 1%, a large resistor (~ 500 k) may be connected in parallel with either one in order to correct any imbalance.

D. Phase Shifters

The discussion of the phase shifters given by Berg is misleading (ref. 30, p.29). In practice, it is only necessary to know that the reference and sample channels each shift phase by 90°, and that the net fluorescence shift can never retard the phase by more than 90°.

The 1 k helipot on both channel shifters was changed to 10 k, and the use of the 900Ω/step switches eliminated. Since a phase reading could never be reproduced to better than ± .002 in tan $\frac{\theta}{2}$, the old arrangement introduced a non-significant figure in the readings.

Several checks were made on the phase shifters to check their calibration. The procedure was first to insure that the product RC was identical in both channels; and second, that the sum of the phase shifts of the channels was 180°.

The RC product was checked by "tracking" one shifter against the other. To do this, another variable phase shifter was introduced into the reference channel((ref. 30, p.12), this circuit was modified to work at 1 kc), and measurements made with a 1 kc 15v p-p signal from the signal generator. The arrangement is shown in Fig. 12. Both shifters were set at "0" and the phase meter zeroed with the auxiliary shifter. An increase in phase by the reference helipot was matched by an increase in phase by the sample helipot sufficient to zero the meter. Were both

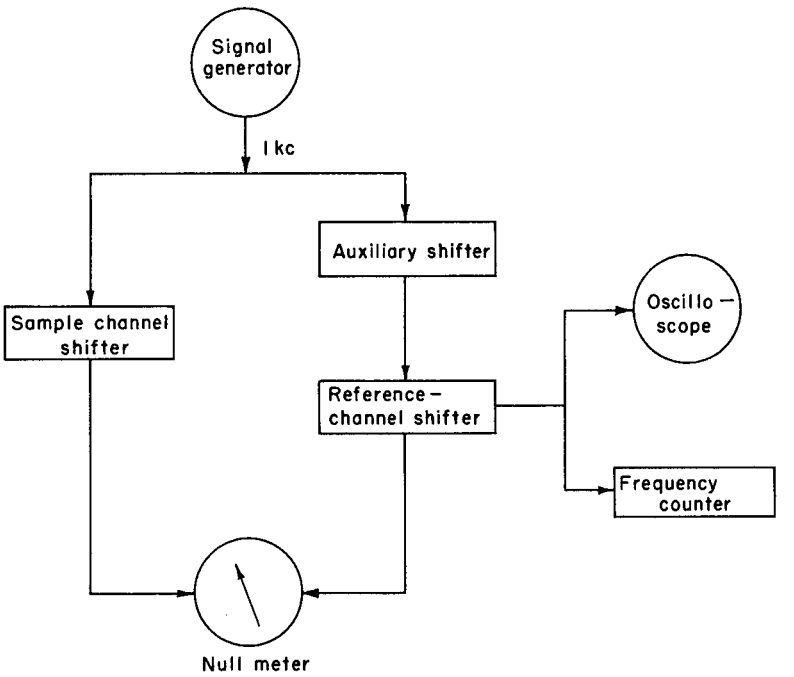
Signal generator
1 kc
Auxiliary shifter
Sample channel shifter
Oscillo-scope
Reference-channel shifter
Frequency counter
Null meter
MU-36900

Fig. 12

helipots identical, the same reading on both duodials would zero the meter. The results are shown in Table I. The maximum deviation is just the rated 0.2% linearity of the potentiometers.

Table I.

	Start		End
Ref. Duodial	0	400	1000
Sample Duodial	0	401	1002

The total phase shift was measured with the null meter, and by observing Lissajou figures on the oscilloscope. To check the null meter shift, the auxiliary shifter had to be changed to the sample channel in order to zero the meter. The results of the total shift averaged to $180.0 \pm 0.2°$. The oscilloscope measurements were made with the "scope" outputs on the reference and sample shifter chassis connected to the vertical and horizontal plates, and the phase between $y = x$ and $y = -x$ recorded. The average of several measurements gave $179.4 \pm 0.4°$ as the total shift.

Tracking errors can be remedied by small trimmer capacitors in one or the other channel. Referring to Table I, a low value at the end of the sample duodial would mean that C was too large in the sample channel; i.e., it was matching a given shift in the reference channel with a smaller R.

However, measuring the same RC for the two channels does not mean that <u>that</u> RC will give a 180° phase shift. It the total shift is less, say 175°, then C is too large in <u>both</u> channels, and an equal capacitance must be removed from each channel, and vice-versa.

To avoid the tracking correction, it might be useful to match identical helipots by accurately measuring their resistance on a General Radio R-L-C bridge. Pairs of pots with resistances to ± 0.1% of each other may then be selected. Both procedures were used in the present work.

While these checks were being made, it was found that the phase detector was extremely sensitive to the reference signal amplitude when both reference and sample signals were present. This could result in a change of phase with small changes in the light level during the course of a measurement. The trouble was traced to the clipping diodes in the reference channel, and it was found that removal of the diodes (actually, the diodes in both channels were eliminated) greatly reduced the amplitude sensitivity.

Moreover, the 5 k 1% resistor in the detector from the sample input to ground was absent in the actual circuit, although it was indicated in the schematic. The detector worked equally well with the sample channel diode in and the 5k resistor out, but did not work at all with both the diode and resistor removed. Both the diode and resistor to ground enable current to flow from ground through the meter on the positive half cycles of the input signals.

A detailed analysis of the effect of various components on the amplitude sensitivity of the phase meter was made; viz., what effects the new cathode followers after the phase inverter, the 5 k resistor from "ϕ" Detector Input" to ground, and the clipping diodes, had on the phase reading.

With a 30 v p-p signal, the duodials were set at "0" and the meter zeroed with the auxiliary shifter. The amplitude of each channel was decreased in two stages from 30 v. to 20 v, and 20 v to 10 v with either

the signal generator amplitude control, or the reference and sample channel attenuators (which introduce no phase shifts). Below 10v the meter loses sensitivity and gradually returns to zero.

The phase angle ϕ necessary to re-zero the meter was recorded. The results are shown in Table II, where "R" and "S" refer to the reference and sample signal amplitudes, "CF out" to the bypassing of the cathode follower stage. The reference "Balance 2" control was adjusted with each change.

The pair (c) and (e) show that the 5k resistor has no effect on the amplitude sensitivity. The pairs (a) and (c); (b) and (d) show the marked reduction in amplitude sensitivity with the removal of the diodes. (a) and (d) indicate that the added cathode followers did reduce the amplitude sensitivity, probably by eliminating distorted signals at the detector. The effect of the reference diode is most likely due to its non-linear characteristics, so that a change in amplitude of the higher harmonics at the detector would introduce new phases in addition to the phase shift of the 1 kc component.

1. Direction of the Phase Shift

In order to determine in which direction the phase is shifted by the fluorescing sample, it is convenient to think of the sample as a length of delay cable, for example, which retards the phase of the sample channel. Thus, if a resistance reading R_1 is read on the sample (or reference)channel with the scattering (zero phase) sol in place; and a reading R_2 on the sample (reference) channel with the sample in place, then, $R_2 < R_1$ (or $R_2 > R_1$).

However, in the process of heterodyning the signal from the higher frequency to 1 kc, the oscillator frequency ω_o is always 1 kc greater

TABLE II.

MODE	SAMPLE SIGNAL at 30 v p-p	REFERENCE SIGNAL at 30 v p-p
(a) 5 k IN, CF IN, DIODES OUT (present mode of operation)	R = 20v; 10v ϕ = 0.0°;0.0°	S = 20v; 10v ϕ = 0.2°;0.3°
(b) 5 k OUT, CF OUT, DIODES IN (past mode of operation)	R = 20v; 10v ϕ = 4.2°;11.1°	S = 20v; 10v ϕ = 0.5°;3.8°
(c) 5 k IN, CF OUT, DIODES IN	R = 20v; 10v ϕ = 0.4°;12.6°	S = 20v; 10v ϕ = 0.4°;0.5°
(d) 5 k IN, CF OUT, DIODES OUT	R = 20v; 10v ϕ = 0.4°;0.5°	S = 20v; 10v ϕ = 0.2°;0.4°
(e) 5 k OUT, CF IN, DIODES IN	R = 20v; 10v ϕ = 5.2°;12.6°	S = 20v; 10v ϕ = 0.5°;7.0°

than the modulation frequency ω_s. If the sample photomultiplier signal is A cos $(\omega_s t + \phi)$, and the oscillator signal a cos $\omega_o t$, then the plate current i_p is just

$$i_p = aA \cos(\omega_s t + \phi) \cos(\omega_o t)$$

$$= \frac{aA}{2} \left\{ \cos[(\omega_o - \omega_s) t - \phi + \cos[(\omega_o + \omega_s) t + \phi] \right\}$$

Only the first term in i_p is passed by the filters and amplified, and we see that the sign of the phase is reversed, while its magnitude remains unchanged, in the mixing process. So the phase of the sample channel is actually advanced (or that of the reference channel retarded) by the sample. (This is not the case with the short-lifetime modulation scheme. There, ω_s = 5.206 Mc, and ω_o = 5.205 Mc, so that the phase of the sample channel is always retarded.)

A convenient way of measuring the phase is to zero the meter with one shifter, leaving sufficient range on the second shifter to measure a fluorescent and zero phase on it, so that the net phase shift is the simple difference of the two phases.

Another procedure is to set the sample channel at "0" with the sol in place, and zero the meter with the reference channel. The fluorescent phase can then be read directly on the sample channel with no subtraction necessary. If the meter cannot be zeroed with the reference shifter, then the reference shifter can be set at "1000" and the zero phase balanced with the sample shifter. The complement of the phase shift may then read off the reference shifter.

E. Multiplier Phototube Bases

The wiring of the phototube bases are shown in Figs. 13 and 14. The voltage division for both tubes is for maximum tube gain rather than maximum current. The capacitors in the last dynode stages prevent drops in the dynode voltages with the relatively large currents carried by these stages. The voltage between pin 1 (deflector) and pin 2 (first dynode) on the Amperex tube was varied by a 1MΩ potentiometer to find the point of maximum tube output. This point was with the two pins tied together.

The tuned circuits on the anode are tuned to 99 kc or 359 kc (or 5 Mc when used with the short-lifetime apparatus), and any change in the modulation frequency must be accompanied by a retuning of these filters.

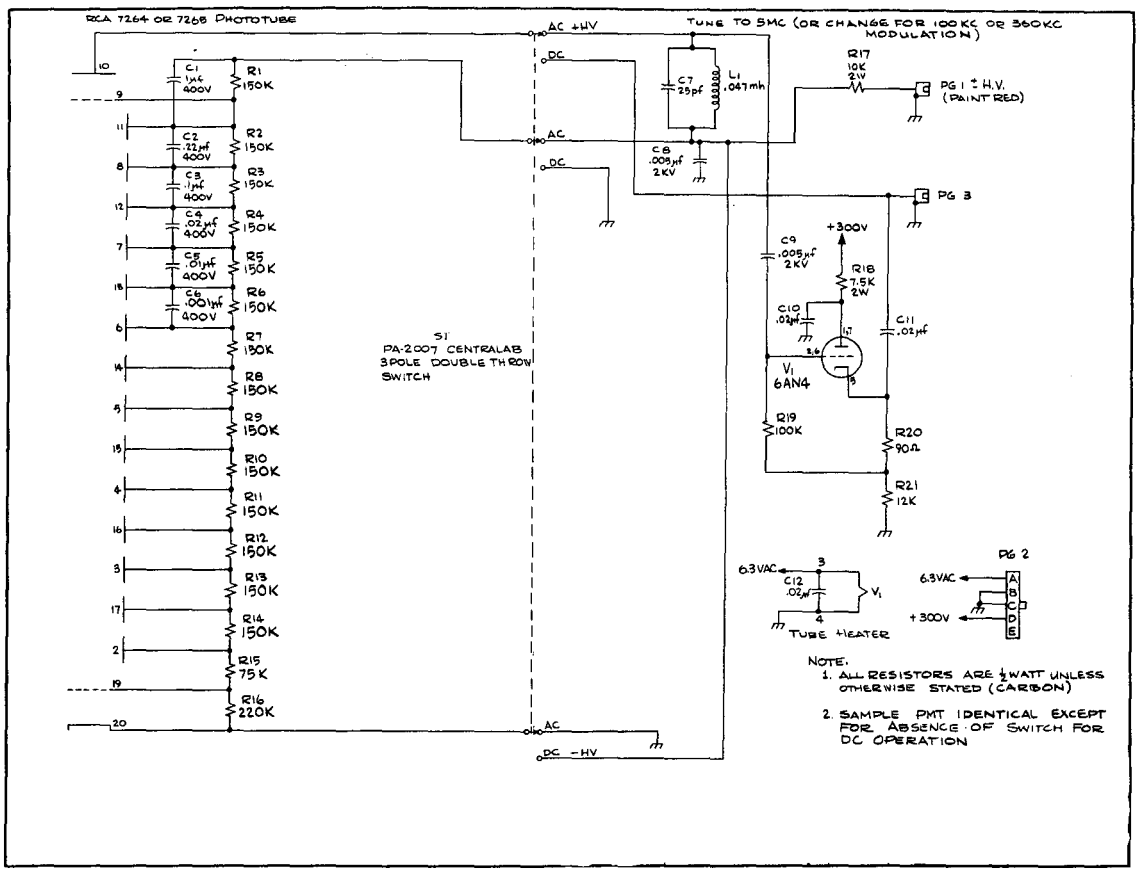

MUB-8933

Fig. 13

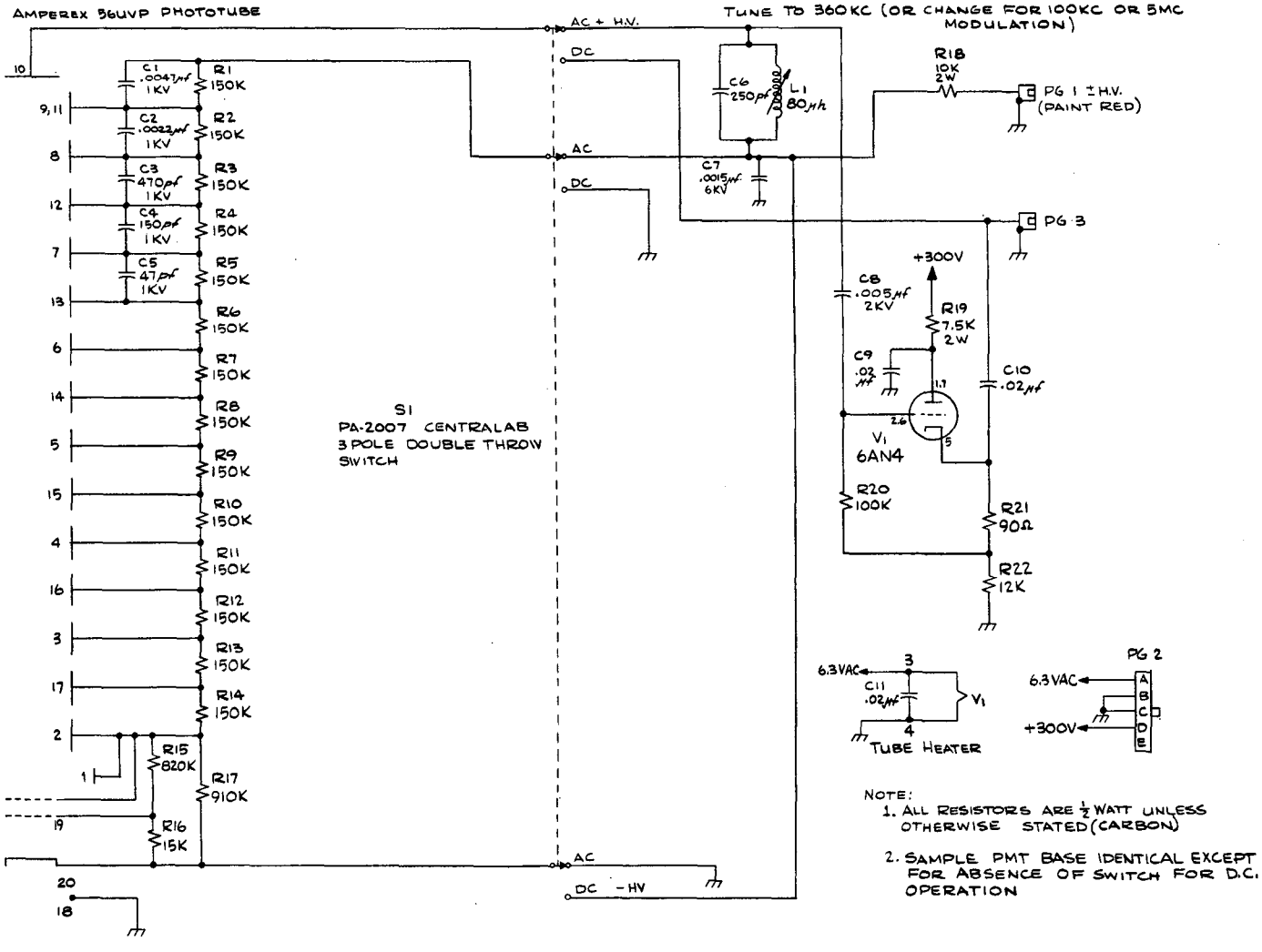

MUB-8625

Fig. 14

III. THE ZERO PHASE

The importance of reproducing the fluorescent geometry when measuring the zero phase was emphasized by Stafford[29] with reference to the 5.2 Mc supersonic grating modulator of the short lifetime apparatus. He observed large variations in phase across the grating-modulated light beam as he moved a samll orifice across the image of the diffraction pattern produced by the tank. He also emphasized the errors that can arise by using merely a glass plate to measure the zero phase.

In the present work with the wheel modulator, the similar variation of zero phase was observed, and the effect was traced back to large inhomogeneities of phase across the light spot from the wheel.

A 2 mm aperture was used to scan a cross-section of the spot approximately 15 mm in diameter. The photomultiplier voltage was held constant, and changes in the light intensity were compensated for by the addition or removal of neutral density filters. Figure 15 shows the relative changes in phase as the aperture was moved across the spot of the modulated Hg 5461Å line.

With the use of the glass plate as the zero phase, 7 degree variations in the "zero phase" could be gotten by focusing only part of the divergent light beam on the photomultiplier face. Only when care was taken to insure that the entire spot fell on the tube face did the zero phase agree to within 0.8° of the phase from the MgO scattering sol.

In all subsequent work a low density (~ 0.1% by weight) MgO sol was used to reproduce the fluorescence geometry. The sol and the fluorescence cell were both single-horned cells of identical dimensions.

To check the phase variations in the light scattered from the sol, the exit window of the sol was masked into top, bottom, right and left

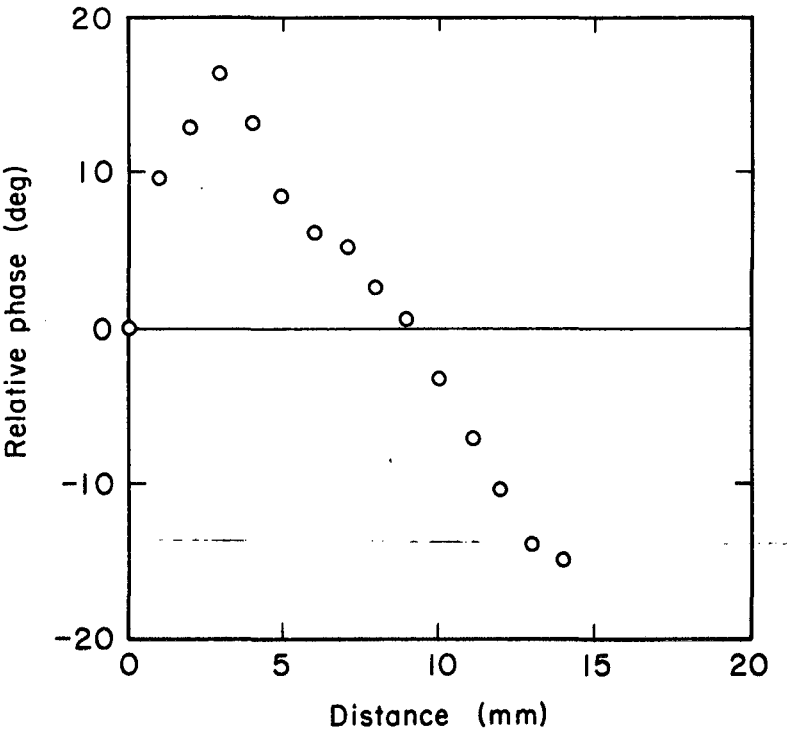

MU-36899

Fig. 15

halves. The phase of each half was measured and found to vary by only 0.4°. Variations in phase with changes in the sol positioning were less than 2°, and this effect was further minimized by reproducing the fluorescent cell positioning with the sol. A given lifetime could be repeated to better than 5% with successive readings of sample and sol phases.

These large phase variations in the light spot are most likely caused by defects in the wheel ruling, and non-parallel wires in the transmission grating (clearly visible to the eye). Together with pincushion and barrel distortions in the lenses, these deviations cause mismatch between the wheel grooves and the grating dark and light lines. Thus, every time a light grating line crosses a wheel groove, rather than being focused parallel to the groove, a 180° phase change is produced. This mismatch is also seen in the shape of the Moiré fringes. These fringes are not straight lines, but are noticeably zig-zagged, showing the variation in relative spacing between the wheel and grating lines. (The analogous effect would be seen in the supersonic grating where reflections of the standing waves would cause a compression to appear in place of a rarefaction.) The net result after the light is gathered from the wheel is some average over the spot diameter of light with phases varying between 0° and 180°.

IV. WHEEL MODULATOR OPTICS AND FOCUSING

The optical system was considerably simplified over the arrangement used by Berg (ref.30, p.7). The projector lens arrangement was found to be unnecessary, and the three lenses were replaced by a single thin quartz lens, with an estimated increase in transmission of ~25%. The optical arrangement is shown in Fig. 16.

The grating G was made by wrapping No.37 (4.5 mil) copper wire on an expandable aluminum frame with grooves cut 10 mil apart. After wrapping the wire was epoxied to the frame, and stretched. The grating was equivalent to the previous celluloid film grating used, and had the added advantage of transmission in the ultraviolet.

The grating is illuminated by L_1 which collimates the light from the lamp. The illuminated grating is the object of the lens L_2 which focuses the image on the wheel. In order to get the necessary reduction of the 100 lines/inch of the grating to the 500 lines/inch of the wheel, it is necessary to have $s'/s = 1/5$.

A convenient focusing procedure is to set s' at f_2, the focal length of L_2, and move G to $5f_2$, with L_1 as close to G as possible to get the maximum amount of light through the grating. This constitutes a crude focus, and a finer one is gotten by tilting the grating in its holder and looking for Moiré fringes on the wheel. The presence of these fringes indicates that the image of the grating spacings is comparable to the wheel spacings. L_2 and G should then be moved until the fringes broaden and disappear. Final adjustment of L_2, G, the grating tilt, and the lamp positioning is made by locking the wheel in and maximizing the 359 kc or 99 kc signal.

The percent modulation of the reflected light is measured by rotating the wheel by hand, and measuring the maximum and minimum DC current with the reference PMT and the oscilloscope. If these are I_{max} and I_{min}, then

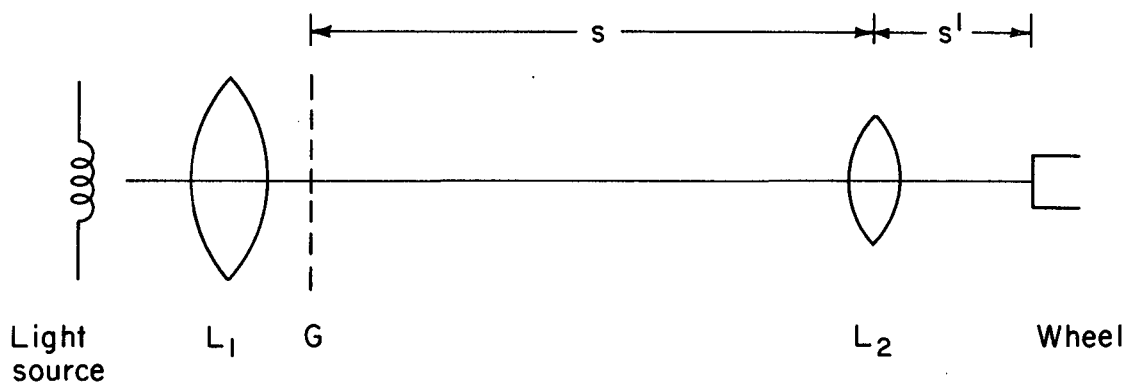

Fig. 16

$$\% \text{ MOD} = \frac{I_{max} - I_{min}}{I_{max} + I_{min}} \times 100.$$

The percent modulation depends upon the quality of the focus, and also upon the spectral purity of the line being focused. If several wavelengths are present in the light from the lamp, only one will be exactly in focus; the others will remain somewhat out-of-focus due to chromic aberrations in the lenses, and these wavelengths will appear as scattered light, reducing the percent modulation. In practice, the percent modulation varied from 15% for the mercury 2537Å line filtered through a $NiSO_4$ - $CoSO_4$ solution, to 55% for the sodium D lines, isolated by a narrow band-pass interference filter.

In order to eliminate effects of the wheel's curvature, the focused spot on the wheel should be kept small. A simple calculation shows that the center and edges of the spot will be in focus if the spot width is kept less than 1 cm. At widths greater than this, the curved wheel will no longer appear to be flat, and out-of-focus light at the spot edges will reduce the percent modulation. The spot size was adjusted by masking the transmission grating to a 2 cm × 3.3 cm rectangle. The masking caused only a small decrease in modulated light intensity.

For work at the 2537Å line, L_2 was an f/1.5 fused quartz lens, with f_2 = 1.5"; and L_1 was f/1.6 fused quartz with f_1 = 4". At the visible wavelengths (6040Å to 5011Å), L_2 was replaced by an f/2.5 Tessar camera lens with f_2 = 2". In both cases an f/1.2 3" focal length quartz lens was used to focus the light from the wheel onto the sample.

V. LIFETIME OF THE MERCURY $^3P_1$-$^1S_0$ λ2537Å TRANSITION

Because of the large phase inhomogeneity in the modulated light beam, it became clear that large errors in lifetimes could result from improper measurements of the zero phase.

Measurement of the lifetime of the mercury $^3P_1$ state was selected as a good check on the over-all functioning and accuracy of the apparatus. Mercury has several advantages that (a) it is relatively volatile, and sufficient vapor density can be obtained without externally heating the absorption cell; (b) its lifetime is well known via measurements by a variety of techniques; (c) there are good sources of Hg 2537Å light available; and (d) sufficient phase shift can be obtained at the modulation frequencies available. The λ3261Å intercombination line of cadmium may also serve as a lifetime check, although it lacks in (a) above.

A. Experimental Procedures

The resonance absorption cell was made of fused quartz with a single Wood's horn to minimize scattering of the incident light. The cell was evacuated to 2×10^{-5} torr for 24 hours, during which time it was torched to 500-600°C several times for 10 minutes in order to facilitate outgassing. The system was then bled with helium, and several drops (~ 5g) triply distilled mercury[24] introduced in air into the cell. The entire system was again evacuated to 2×10^{-5} torr and the mercury in the cell was sealed off at approximately 1×10^{-4} torr.

After seal-off, the mercury in the cell was carefully distilled into the stem, and the cell coated with Aqua-dag. A small uncoated opening was left in the horn to allow transmission of unabsorbed exciting light.

The light source was a General Electric Germicidal Lamp powered by a Burdick Diathermy Machine. The diathermy output power was set to give a maximum fluorescence signal from the mercury atoms at reasonable lamp intensities. The microwave source gave an extremely stable light output, with none of the 60 cycle ripple on the 1 kc signals gotten with AC power supplies. The 2537Å line was filtered with a 5 cm path of 0.35M $CoSO_4$ - 2.0M $NiSO_4$ solution.[31]

Temperatures of the stem were maintained with a Haake Type F thermal regulator which regulated to ± 0.02° from - 30°C to 0°C. All temperatures were measured with a Fe-constantan thermocouple in conjunction with a Leeds and Northrup potentiometer. The thermocouple read 0.0° for ice and - 199.5° for liquid nitrogen (B.P. - 199.8°).

The actual absorption of the exciting line from the germicidal Lamp by the mercury in the cell can be measured by placing the PMT directly behind the Wood's horn and facing the incoming beam passing through the cell. The mercury in the cell is frozen out by placing a dewar of liquid nitrogen on the finger, and the sample PMT voltage is adjusted to give a 15 v p-p 1 kc signal. As the finger is gradually warmed up, the amplitude of the sample signal decreases as mercury atoms in the light path absorb and reradiate the exciting line. If the exciting line is greatly self-absorbed or Doppler broadened, there will be only a small fraction of light absorbed by the mercury atoms in the cell with their narrow Doppler profile. Also, if an absorption cell has been wrapped with heating wires in order to get vapor pressures in the cell at temperatures higher than room temperature, this procedure will indicate if there are any "cold-spots" in the cell where the vapor is condensing. In the present experiments, 65% of the exciting line was absorbed by the mercury atoms near room temperature.

During the actual fluorescence runs, rather than relying on the cell's attaining equilibrium, a method was adopted which did not require knowledge of the exact vapor density in the cell. The ratio of the fluorescence intensity to the scattered light intensity (I_f/I_s) was measured at each phase reading, and the lifetime (corrected for scattered light) was plotted against this ratio, rather than against temperature. (The temperature measurements, however, did give enough indication of the partical density to allow an estimate of when to expect increases in the lifetime due to entrapment.)

B. Measurement of the Fluorescence and Zero Phases

The thermal regulator maintained the cell at temperatures from - 30°C to 0°C, and changes in the fluorescence intensity were compensated for by changes in the PMT voltage necessary to maintain a 15 v p-p 1 kc signal. A resistance reading on the Duodial (the fluorescence phase) which gave a null on the meter was recorded.

After each fluorescence phase reading, the zero phase was measured using a dilute MgO scattering sol in an identical pyrex cell which had quartz entrance and exit windows held in place by Apiezon black-wax. The MgO sol was prepared by filtering a suspension of MgO in water several times through glass wool to remove large particles. The sol was shaken thoroughly before each zero phase reading, and its concentration was such as to give amplitudes of scattered light nearly equal to the amplitudes of fluorescence signals observed.

The procedure of measuring the zero phase after each fluorescence measurement, rather than after all the fluorescence phases at all the desired temperatures had been measured, was adopted because of gradual drifts in the zero phase with time. The zero phase readings taken after

each set of fluorescence phase readings were consistently higher than those taken before by as much as 5-8%. The cause of this phase drift could not be found, and was present even after the apparatus was allowed to run in lock for several hours. These shifts are gradual, however, and one may take a zero phase reading every 20 minutes, instead of after each fluorescence phase reading.

In order to obtain a 15v signal with the sol-scattered light (which was always more intense than the fluorescence intensity) at the same PMT voltage settings used in the fluorescence phase reading, wire screens of different mesh were used to attenuate the scattered light. In this way, fluorescence and zero phases were measured at equal signal amplitudes without introducing phase shifts with changing PMT voltages. The attenuation of each wire screen was calibrated by focusing the 2537Å line on the PMT face, and measuring the DC output on an oscilloscope as each mesh (and combinations of meshes) was inserted. The "neutral density filter" rating of each mesh is then just $\log_{10}\left(\frac{i}{i_o}\right)$ where i and i_o are the PMT currents with and without the wire screen in place.

All light levels were measured with Amperex 56 UVP phototubes having a "U" spectral response.[32] The divider chain was wired for maximum gain, as shown in Fig. 15. Applied voltages never exceeded 1800 volts, and all the fluorescence data were taken with the sample channel voltages between 1200 and 1550v, and the reference channel between 730 and 760v. The dark current for both tubes was 30 - 40 μA at 1700v.

C. Scattered Light Correction

The scattered light correction to the lifetimes is that given by Berg (ref. 30, p.83) with one important exception. He calls N the opti-

cal noise signal corresponding to $\tau = 0$. There were cases where the "scattered" light from the cell with the mercury frozen out did not reproduce the zero ($\tau=0$) phase from the sol. A possible explanation for this may be due to the fact that the measured DC amplitude (as seen on the chart recorder) of the light from the cell is made up of random pulses (from ohmic leakages, shot noise, etc., in the PMT) which contain no phase information, as well as true scattered light from the cell itself. Thus, a noisy 15v p-p signal might contain only a rectified 10v p-p scattered light amplitude, the reaminder consisting of rectified noise pulses.

The light scattered off the sol, however, does not consist of dark current pulses, and will register a definite phase of scattered light corresponding to $\tau = 0$. The signal detected by the sample photomultiplier will be the sum of a fluorescence signal I_f of phase $\Delta\phi$, and a scattered light signal I_s of phase $\Delta\phi_o$. Letting the amplitude and phase of the sum be I and $\Delta\phi_m$, we have

$$I \cos(\omega t - \Delta\phi_m) = I_f \cos(\omega t - \Delta\phi) + I_s \cos(\omega t - \Delta\phi_o) \quad (3)$$

where $\Delta\phi_m$ is the measured phase shift, while $\Delta\phi$ is the true phase shift in the absence of scattered light.

Equation (3) may be solved in terms of the ratio $\left(\frac{I}{I_s}\right)$ or $\left(\frac{I_f}{I_s}\right)$. Solving for the former we get, after expanding the sum-of-angles and equating the sin ωt and cos ωt coefficients,

$$\tan\Delta\phi = \frac{(I/I_s)\tan\Delta\phi_m - \dfrac{\sin\Delta\phi_o}{\cos\Delta\phi_m}}{(I/I_s) - \dfrac{\cos\Delta\phi_o}{\cos\Delta\phi_m}} \quad (4)$$

If the zero phase $\Delta\phi_o$ is 0°, then Eq. (4) becomes

$$(\tau/\tau_m) = \frac{(I/I_s)}{(I/I_s) - \frac{1}{\cos\Delta\phi}} \qquad (5)$$

where the relation $\omega\tau = \tan\Delta\phi$ was used.

The quantity I_s can be measured by freezing the sample from the cell and noting the PMT voltage, while I is the intensity of the fluorescent and scattered light signal at some lower PMT voltage. The ratio (I/I_s) can be gotten from the relative gain of the PMT between these two voltages.

An alternate procedure used in the present work is to solve for the ratio (I_f/I_s) from Eq. (3), and we get that

$$\tan\Delta\phi_m = \frac{(I_f/I_s)\tan\Delta\phi + \frac{\sin\Delta\phi_o}{\cos\Delta\phi}}{(I_f/I_s) + \frac{\cos\Delta\phi_o}{\cos\Delta\phi}}$$

and if $\Delta\phi_o = 0°$,

$$\tau/\tau_m = \frac{(I_f/I_s) + \frac{1}{\cos\Delta\phi}}{(I_f/I_s)} \qquad (6)$$

The quantities I_s and $I \doteq I_s + I_f(T)$ are measured as above, and the two photomupliplier voltages are converted into neutral density filter values by measuring the relative gain of the PMT between the two voltages. This is easily done by attenuating a scattered light signal from the sol while increasing the PMT voltage. A plot of N.D. vs voltage then gives the desired gain.

The sequence of measurements can be seen in Fig. 17. The scattered light in the cell measured at V_2 has an amplitude $I_s 10^{\Delta ND}$ where $10^{\Delta ND}$ is the gain of the PMT between V_1 and V_2, so that

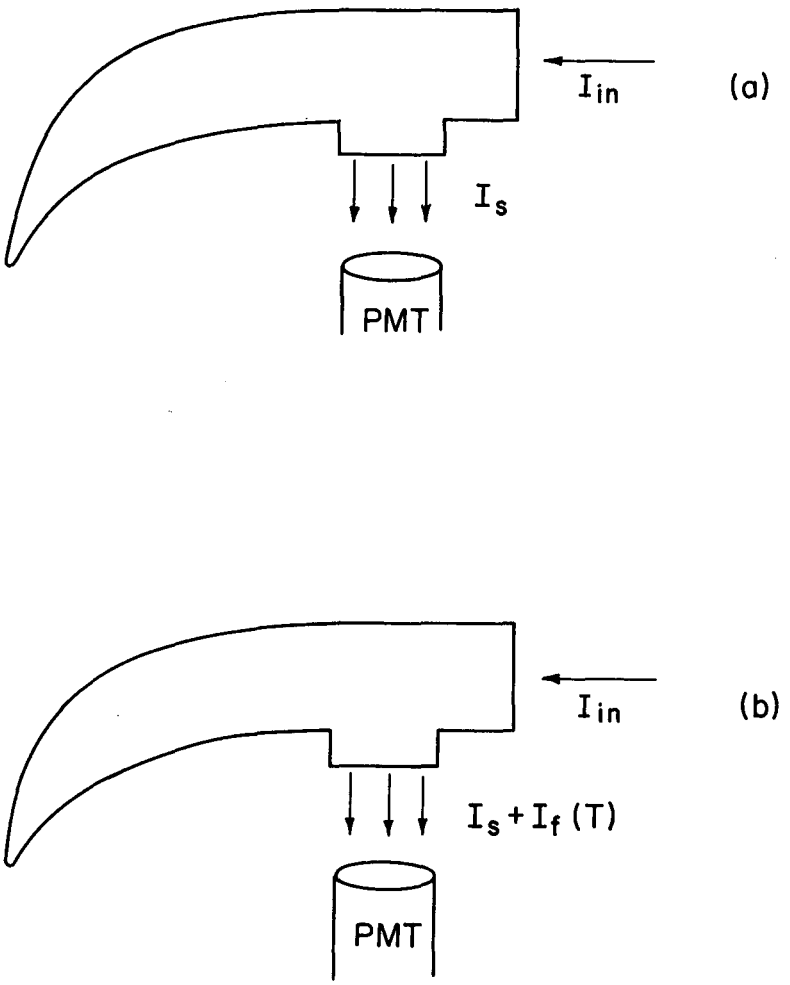

Fig. 17

$$I_s + I_f(T) = I_s 10^{\Delta ND}$$

or

$$\frac{I_f(T)}{I_s} = 10^{\Delta ND} - 1$$

The scattered light correction in Eq. (6) varies from 25% to 2% for (I_f/I_s) = 4 to 50 and $\Delta\phi_m \sim 10°$. Below (I_f/I_s) = 4, the uncertainty in ΔND (approx. ± 0.2) made the uncertainties in τ/τ_m large. The value of ΔND for these low fluorescent light levels was changed within the experimental uncertainty to prevent the low temperature end of the plot from swinging up (τ/τ_m too large, ΔND too small, less scattered light in cell than measured) or down (vice-versa).

In each run, the cell was allowed to equilibrate at 0°C for 10 minutes in order to obtain (I_f/I_s) at a known particle density. The (I_f/I_s) of each run were scaled to the same value at 0°C, since the corrected 0° lifetime should be the same for all the runs, regardless of the scattered light in the cell.

The final results are shown in Fig. 18. The lifetime was obtained from the level region between (I_f/I_s) = 3 to 10, and was (1.10 ± 0.05) X 10^{-7} sec. This is in good agreement with the values of Garret and Webb (1.08 ± 0.01 X 10^{-7} sec)[33] gotten from modulated electron excitation and optical detection; and with the absorption measurements of Kopfermann and Tietze (1.08 X 10^{-7} sec);[34,80] and also with a recent value cited by Lurio from zero field crossing measurements of (1.16 ± 0.02) X 10^{-7} sec.[35]

D. Entrapment in Mercury Vapor

In order to justify the choice of the flat region as the true lifetime, and to explain the gradual slope to the τ vs (I_f/I_s) plot, some

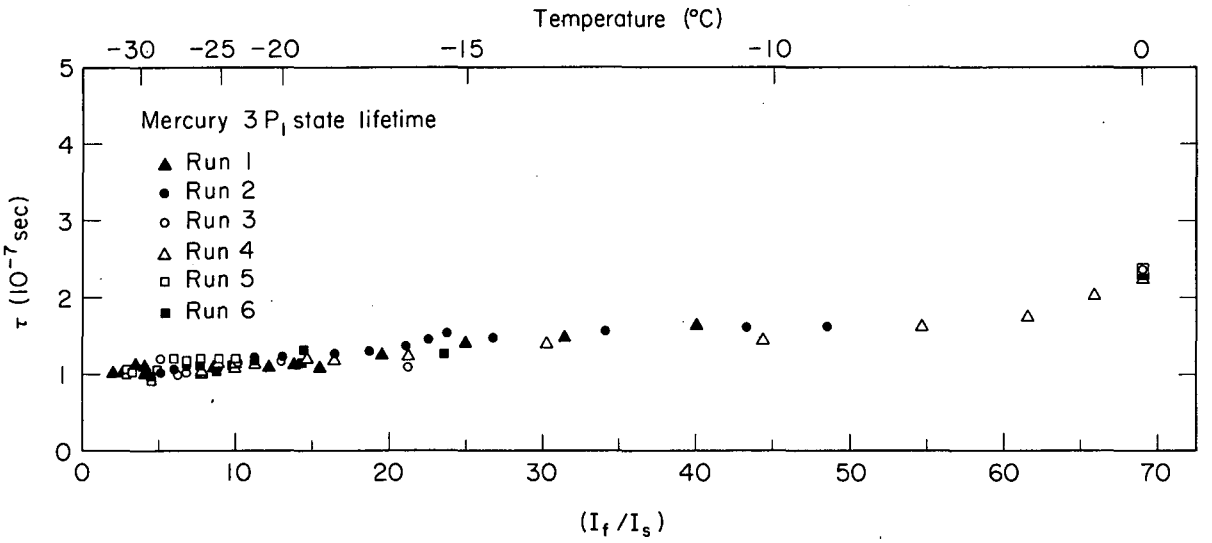
Temperature (°C)
-30
-25
-20
-15
-10
0
Mercury 3 P1 state lifetime
Run 1
Run 2
Run 3
Run 4
Run 5
Run 6
τ (10⁻⁷ sec)
0
1
2
3
4
5
0
10
20
30
40
50
60
70
(If /Is)
MU-36892

Fig. 18

measure of the temperature at which entrapment could be expected had to be obtained.

One would expect to see some effects of entrapment when approximately 10% of the center of the resonance emission line was reabsorbed by other mercury atoms in the path, L, between the emission point and the PMT. The curve-of-growth method given by Kopfermann and Wessel[36] was used in this case to determine when the most abundant isotope, Hg^{202}, would have its emission line reabsorbed by other Hg^{202} atoms.

If the resonance radiation from a resonance lamp is passed through an absorption cell containing the same gas that is in the lamp, then the fraction absorbed, A, of the line can be defined as (ref. 3, p.118),

$$A = 1 - \frac{\text{transmitted radiation}}{\text{incident radiation}},$$

or, integrating over all absorption frequencies,

$$A = \frac{\int_{-\infty}^{\infty} [I_o(\nu) - I(\nu)] \, d\nu}{\int_{-\infty}^{\infty} I_o(\nu) \, d\nu} \tag{7}$$

If we assume that the emission profile of the resonance lamp, and the absorption profile of the absorbing gas are both Doppler broadened, then we may write for the incident and absorbed intensities at a frequency ν

$$I_o(\nu) = I_o(\nu_o) \, e^{-\alpha^2(\nu-\nu_o)^2}$$

$$I(\nu) = I_o(\nu) \, e^{-k_\nu \cdot L} \tag{8}$$

$$k_\nu \cdot L = Ce^{-\beta^2(\nu-\nu_o)^2}$$

where k_ν is the absorption coefficient of the absorbing gas, α and β are the Doppler widths (in sec) of the exciting and absorbing lines, respectively, and L is the total absorbing path of the second cell, with $C = \sqrt{\pi}\ \frac{e^2}{mc}\ NL\ f\ \beta$ (e-electron charge, m-electron mass, N-particle density, f-oscillator strength of the transition, c-speed of light).

Substituting Eq. (8) into Eq. (7), we get

$$A = \frac{\int_{-\infty}^{\infty} I_o(\nu)\ \left[1 - e^{-k_\nu \cdot L}\right] d\nu}{\int_{-\infty}^{\infty} I_o(\nu)\, d\nu} \qquad (9)$$

We can expand Eq. (9) and integrate term-by-term to get finally

$$A = \sqrt{\pi}\ \frac{e^2}{mc}\ NfL\alpha \left[\frac{1}{\sqrt{1 + \frac{\alpha^2}{\beta^2}}} - \frac{C}{2!\sqrt{2 + \frac{\alpha^2}{\beta^2}}} + \frac{C^2}{3!\sqrt{3 + \frac{\alpha^2}{\beta^2}}} + \cdots \right] \qquad (10)$$

The first term in the series of Eq. (10) represents absorption proportional to the particle density, N, of Hg^{202} atoms, while the second term varies as N^2. Thus, as the particle density is increased, the negative second term tends to diminish the absorption A. Or, as the concentration of atoms increases, the total line absorption increases less rapidly since the center of the resonance line is being absorbed out.

It is useful to determine at what particle density the second term in Eq. (10) becomes approximately 10% of the first. At this density, the mean free path of the photons will be of the order of the distance between the emitting point and the exit window, so that many more of the photons

will be entrapped by the time they reach the photomultiplier.

The Doppler widths α and β are given by

$$\alpha = \frac{2\sqrt{R\ell n 2}}{\lambda_o}\sqrt{\frac{T^{\alpha}}{M}}$$

$$\beta = \alpha\sqrt{\frac{T^{\alpha}}{T^{\beta}}}$$

where T^{α} is the operating temperature of the Germicidal Lamp, estimated as 400°K; and T^{β} the temperature of the absorbing species, taken as 300°K. The corresponding Doppler widths are then $\alpha = 8.28 \times 10^{-10}$ sec (40.3mK), $\beta = 9.56 \times 10^{-10}$ sec (34.9 mK), and $\frac{\alpha}{\beta} = 0.866$. Equation (10) then becomes, with f taken as 0.0264 (corresponding to $\tau = 1.10 \times 10^{-7}$ sec),

$$A = 1.90\,(10^{-12}N)\,[0.755 - 0.661\,(10^{-12}N) + 0.412\,(10^{-24}N^2) + \ldots] \quad (11)$$

where N is the number of Hg^{202} atoms given by

$$N = 0.3\,N_{TOT} = (0.290 \times 10^{19})\,(P/T) \text{ atoms/cc} \quad (12)$$

the factor 0.3 being the isotopic abundance of Hg^{202}.[37]

The particle densities were calculated from the vapor pressure data of mercury between 200.0°and 298.15°K according to the relation

$$-R\,\ell n\,P = \frac{\Delta H^{\circ}_{v\,298}}{T} - \Delta\,\frac{F^{\circ}_{T} - H^{\circ}_{298}}{T} \quad (13)$$

where $\Delta H^{\circ}_{v\,298}$ is the standard heat of vaporization for mercury, and is taken as 14,652 cal/mole from Busey and Giauque's data.[38,39] The free energies F°_{T} for intermediate temperatures were obtained by a linear interpolation of the free energies at 200.0° and 298.15°K. The heat

capacities are again taken from Busey and Giauque (15-330°K), and Eq. (13) becomes

$$R \ln P = \frac{14,652}{T} - 23.622 + \frac{0.562}{98}(298-T) \qquad (14)$$

With the particle densities calculated from Eqs. (12) and (14) it is found that the absorption A is 10% at approximately 242°K where P = 3.58×10^{-6} torr and Nf = 1.90×10^{9} atoms/cc. The second term in Eq. (11) becomes 10% of the leading term at approximately 246°K where P = 9.20×10^{-6} torr and Nf = 2.86×10^{9} atoms/cc. These two temperatures correspond to (I_f/I_s) of approximately 8 and 12 respectively.

This then shows that the lifetimes from $(I_f/I_s) = 3$ to 10 will be relatively unentrapped. As the vapor density increases, the most abundant mercury isotope, Hg^{202}, will begin to entrap, giving a gradual slope to the τ vs (I_f/I_s) plot which increases as the other isotopic concentrations increase.

VI. LIFETIMES AND CROSS SECTIONS OF I_2 FLUORESCENCE FROM VARIOUS v' REGIONS OF THE $B^3\Pi_{0+u}$ STATE

A. Iodine Distillation

The same single-horned quartz cell used in the mercury lifetime measurements was used in the I_2 work. The temperature range covered was - 4°C to 24°C (20.2μ to 282μ I_2 pressure) and the zero phase was measured with a dilute MgO scattering sol. The concentration of the sol was adjusted so that the scattered light amplitude was equal to the largest fluorescence amplitude from the iodine cell.

The empty quartz cell was evacuated to 1×10^{-5} torr, and heated to 600°C to drive off water and adsorbed gasses from the cell walls. The system was then bled with helium, and the cell removed and filled with Baker reagent grade I_2 in a dry-box flushed with dry nitrogen, and containing $CaSO_4$ ("Drierite") and NaOH pellets as dessicants. The I_2 was introduced into the long stem only, and was distilled into the cell at a pressure of 8×10^{-5} torr. After 10-15 minutes, the cell was sealed off at approximately 5×10^{-5} torr.

Cell temperatures were controlled with the Haake Thermoregulator, and no difficulty was had in varying the I_2 pressure in the cell with changes in the finger temperature; and in reproducing data points by starting from low temperatures and heating to room temperature, and then reversing the process. No slow decrease in τ with time as mentioned by Berg (ref. 30, p.78) was observed, since his cell was sealed with a greased stopcock which leaked slowly.

B. Light Sources and Filters

Excitation of the I_2 fluorescence was accomplished with a variety of light sources which included Osram Lamps, a mercury 100 watt AH_4 lamp, and a commercial 600 watt G.E. "Sun Gun" (used for floodlight illumination) which served as a continuum light source. The "Sun Gun" was operated on 60 cycle AC, the Osram Lamps on 50-100 cycle square wave, and the mercury lamp on DC.

Scattered light from the cell was reduced to a minimum by using Kodak Wratten filters (except for Na D line excitation where a Dydimium filter was used) to separate the fluorescence from the exciting line. Several Wratten filters were tested at each wavelength, and the one giving the maximum (I_f/I_s) was used. These filters were found to be superior to a series of blue and red-edge interference filters[40] also tested.

All of the exciting atomic lines and continua were isolated by Baird Atomic interference filters which showed no transmission away from the peak from 2500-7000Å. The full width at half and 10% maximum, and the peak wavelength of these filters are presented in Table III along with other light source data.

C. Scattered Light Correction

The scattered light correction when filters are used to block the exciting light is slightly different than shown in Fig. 7. In measuring the ratio (I_f/I_s) at a particular temperature, it is necessary to know the fraction of scattered light that is transmitted by the filter. If x designates the filter used (No. 21, 23A, dyd., etc.) then $I_{s,\,cell}^{x}$ is the fraction of light scattered from the cell which is transmitted by filter x. The following procedure is used to get the quantity of interest $(I(T)_{f,cell}^{x} / I_{s,cell}^{x})$.

TABLE III.

Peak Wavelength of Filter (Å)	Full Width (Å) at Half Max.	Full Width (Å) at 10% Max.	Blocking Filter (Wratten No.)	Light Source	Mode of Operation
6040	87	153	33	Sun Gun	AC
5895	58	102	Dydimium Plate	Na Osram; Sun Gun	Square; AC
5592	57	103	23A	Sun Gun	AC
5461	50	98	23A	Mercury AH4; Sun Gun	DC; AC
5277	49	90	21	Sun Gun	AC
5168	48	86	21	Sun Gun	AC
5087	29	58	16	Cd Osram; Sun Gun	Square; AC
5011	28	60	16	Sun Gun	AC

(a) With the filter placed in front of the sample PMT, and the I_2 in the cell frozen out with liquid N_2, the sample PMT voltage is adjusted to give a 15v p-p signal at 1 kc. This amplitude is $I^{x}_{s,cell}$. (b) The cell and filter are removed, and the sol is positioned before the PMT. With the same PMT voltage, sufficient neutral density filters are used to attenuate the sol-scattered light to a 15v p-p signal. The sum of the filters is ND_1, and we have $I^{x}_{s,cell} = I^{o}_{s,sol} \cdot 10^{-ND_1}$. (c) When a fluorescence + scattered light amplitude is measured at a temperature T, its amplitude is again matched by the sol-scattered light, now attenuated to the higher signal amplitude (lower PMT voltage) by neutral density filters ND_{sol}. We then have

$$I^{x}_{s,\,cell} + I(T)^{x}_{f,cell} = I^{o}_{s,sol} \cdot 10^{-ND_{sol}}$$

Using (b), we get the right hand side equal to $I^{x}_{s,cell} 10^{ND_1 - ND_{sol}}$, so that

$$\frac{I(T)^{x}_{f,cell}}{I^{x}_{s,cell}} = \frac{I_f}{I_s} = 10^{ND_1 - ND_{sol}} - 1 \qquad (15)$$

The maximum corrections to the lifetime amounted to 15-20% for the lowest temperature points in the 6040Å excitation while most other corrections varied from 0-5%.

D. Stern Volmer Plots

The transition rate out of the upper state may be represented as a sum of rates due to a radiative decay rate $\frac{1}{\tau_o}$, and a self-quenching rate which is related to the frequency of $I_2 - I_2$ collisions, so that

$$\frac{1}{\tau} = \frac{1}{\tau_o} + Z \qquad (16)$$

The quantity Z is the collision frequency in a uniform gas having a collision cross section σ^2 (the square of the collision diameter), where

$$Z(\text{sec}^{-1}) = 4N\sigma^2 \left(\frac{\pi kT}{m}\right)^{1/2},$$

m is the mass of the iodine molecule, and N is the concentration of I_2 molecules in particles/cm^3. [41] From the ideal gas law, N is just P/kT, so that

$$Z(\text{sec}^{-1}) = 4\sigma^2[\pi/kTm]^{1/2} P$$

Using T = 300° K, the coefficient of P is just $2.264 \times 10^5 \sigma^2 (Å^2) \frac{1}{\text{torr-sec}}$, and Eq. (16) becomes

$$\frac{1}{\tau} = \frac{1}{\tau_o} + (2.264 \times 10^5)\ \sigma^2 P \qquad (17)$$

A plot of $\frac{1}{\tau}$ against the iodine vapor pressure than yields the unquenched or radiative lifetime (equal to $1/\Sigma A_k$, where A_k are the Einstein transition probabilities to all lower states k). as the intercept, and the I_2- I_2 self-quenching collision cross section as the slope.

Vapor pressures for I_2 were derived from a smooth curve drawn through the data of Shirley and Giauque[42] from 273° to 308°K. Pressures at temperatures below 273°K were interpolated from their $-\frac{F^o - H^o_o}{T}$ value of 52.759 kcal/mole at 250°K for $I_2(g)$. The data are presented in Figs. 19 to 29 and the results summarized in Table IV and Fig. 30.

All results were obtained by a least-square fit to the 35-65 points taken at each wavelength. The runs at each wavelength were taken on separate days; and from lower to higher, and higher to lower temperatures.

The maximum spread in lifetimes at the highest temperatures (20-22°) (smallest phase shifts) was 10%, and no systematic trends either due to foreign gas quenching or lack of attainment of equilibrium were seen. The assignment of errors was made by drawing high and low slope lines about the least square lines, taking into consideration the spread in values at each temperature, and are a measure of the random variation of the data in the present experiments. The errors in τ_o are greatest for small value of $1/\tau_o$ (large τ_o), since a given variation in the intercept is a larger percentage of the small intercept value.

TABLE IV.

Wavelength (Å)	v'	No. of Points	$\tau_o(10^{-7}\text{sec})$	$\sigma^2(Å^2)$
6040	8	63	6.79 ± 0.33	73.7 ± 5
5895 (Cont.)	15	42	11.4 ± 0.6	70.0 ± 4
5890 (Na d)	15	37	11.9 ± 0.7	69.4 ± 3
5592	20	61	6.89 ± 0.33	65.3 ± 4
5461 (Cont.)	25	44	7.69 ± 0.3	67.4 ± 4
5461 (Hg Green)	25	39	7.13 ± 0.25	63.0 ± 3
5277	35	56	9.66 ± 0.5	60.0 ± 4
5168	45	58	$24.1 \begin{smallmatrix} +3.3 \\ -2.6 \end{smallmatrix}$	72.7 ± 5
5087 (Cont.)	50	66	$42.2 \begin{smallmatrix} +7 \\ -5 \end{smallmatrix}$	65.8 ± 4
5086 (Cd Blue)	50	48	$53.2 \begin{smallmatrix} +8 \\ -6 \end{smallmatrix}$	78.7 ± 3
5011	~100	42	17.5 ± 1.5	67.8 ± 4

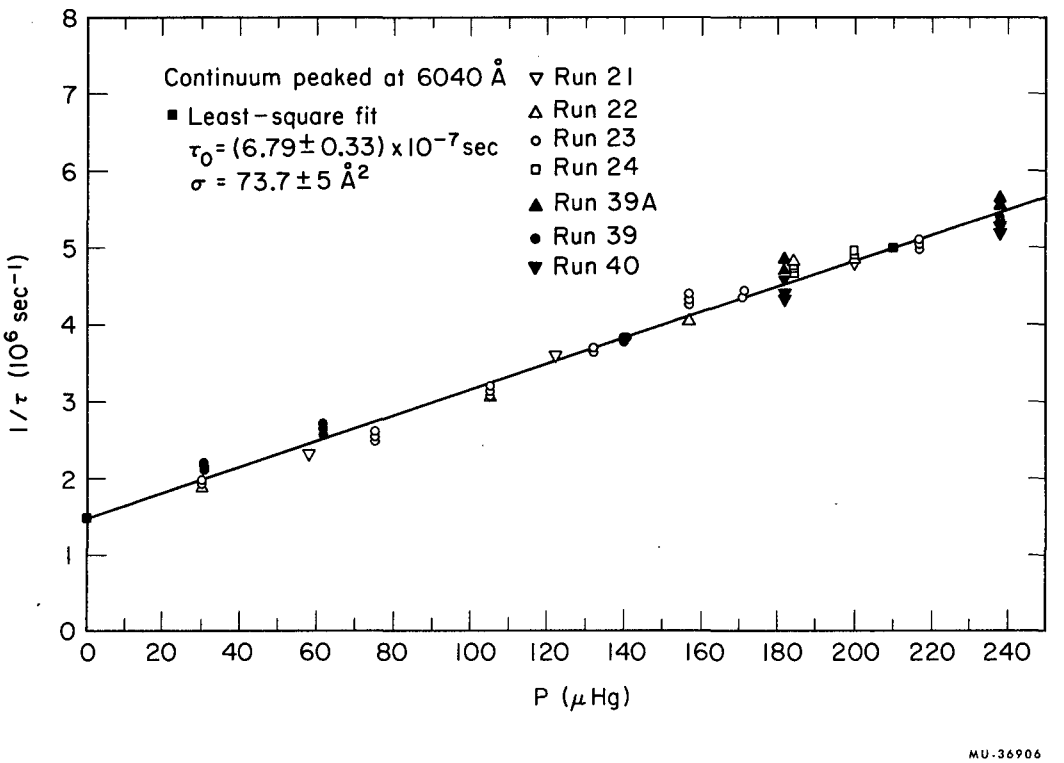
Continuum peaked at 6040 Å
■ Least-square fit
$\tau_0 = (6.79 \pm 0.33) \times 10^{-7}$ sec
$\sigma = 73.7 \pm 5$ Å^2
▽ Run 21
△ Run 22
○ Run 23
□ Run 24
▲ Run 39A
● Run 39
▼ Run 40
$1/\tau$ (10^6 sec^{-1})
P (μHg)
0
1
2
3
4
5
6
7
8
0
20
40
60
80
100
120
140
160
180
200
220
240
MU-36906

Fig. 19

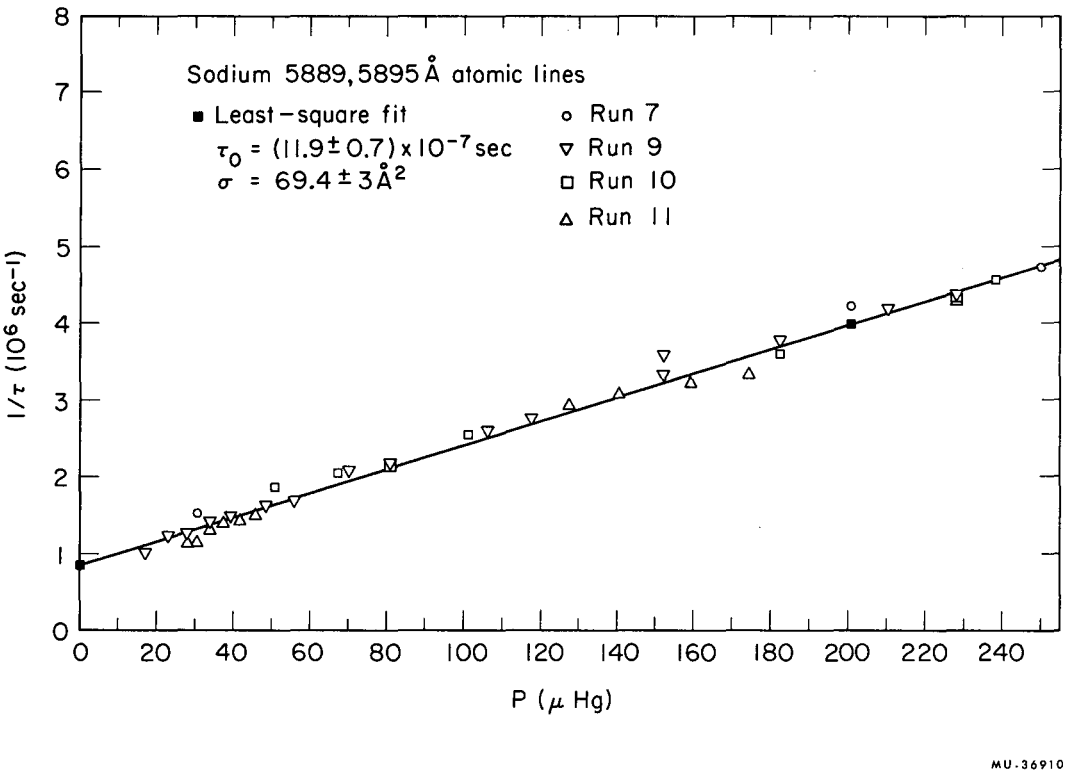
Sodium 5889, 5895 Å atomic lines
■ Least-square fit
$\tau_0 = (11.9 \pm 0.7) \times 10^{-7}$ sec
$\sigma = 69.4 \pm 3 Å^2$
o Run 7
▽ Run 9
□ Run 10
△ Run 11
1/τ (10⁶ sec⁻¹)
P (μ Hg)
0
1
2
3
4
5
6
7
8
0
20
40
60
80
100
120
140
160
180
200
220
240
MU-36910

Fig. 20

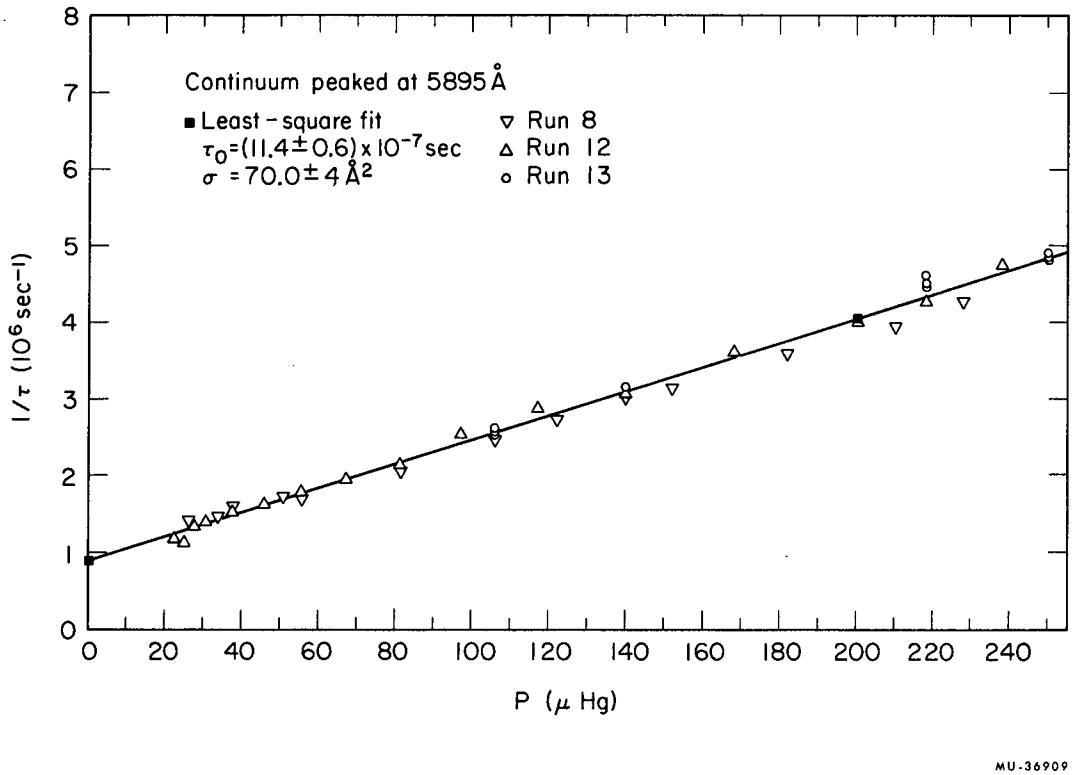
Continuum peaked at 5895 Å
■ Least-square fit
$\tau_0 = (11.4 \pm 0.6) \times 10^{-7}$ sec
$\sigma = 70.0 \pm 4$ Å^2
▽ Run 8
△ Run 12
○ Run 13
$1/\tau$ (10^6 sec^{-1})
P (μ Hg)
0
1
2
3
4
5
6
7
8
0
20
40
60
80
100
120
140
160
180
200
220
240
MU-36909

Fig. 21

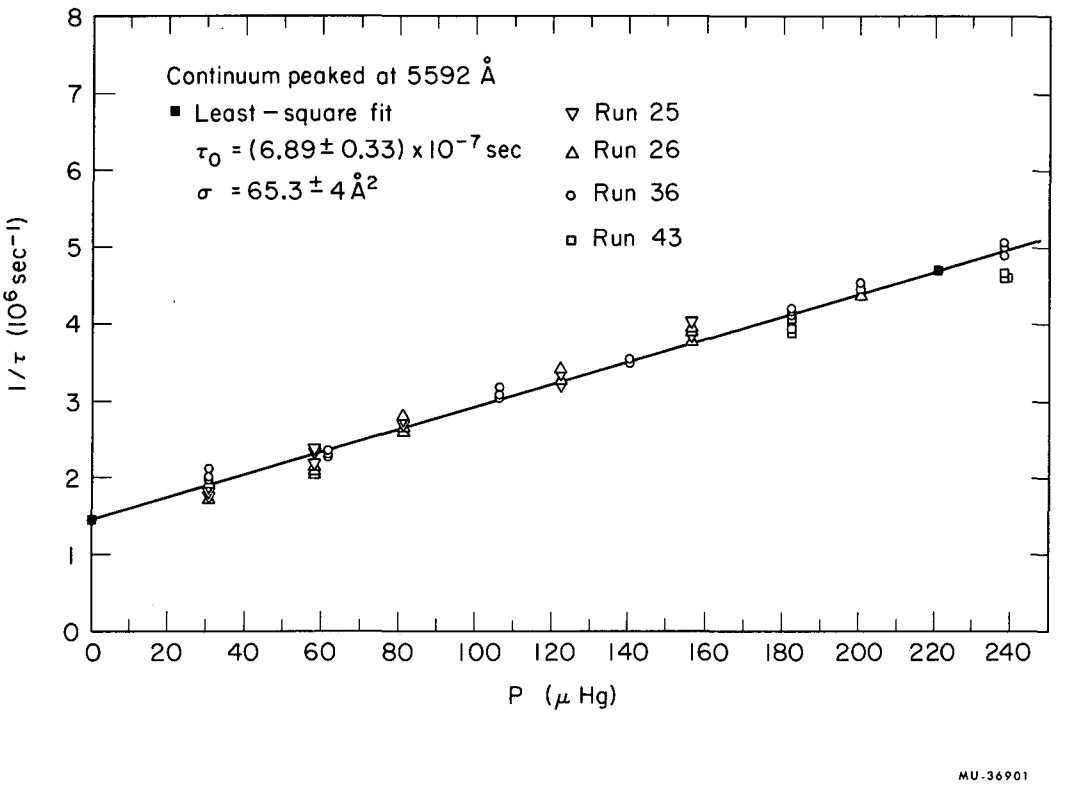
Continuum peaked at 5592 Å
■ Least – square fit
$\tau_0 = (6.89 \pm 0.33) \times 10^{-7}$ sec
$\sigma = 65.3 \pm 4$ Å^2
▽ Run 25
△ Run 26
○ Run 36
□ Run 43
1/τ (10^6 sec^{-1})
P (μ Hg)
0
1
2
3
4
5
6
7
8
0
20
40
60
80
100
120
140
160
180
200
220
240
MU-36901

Fig. 22

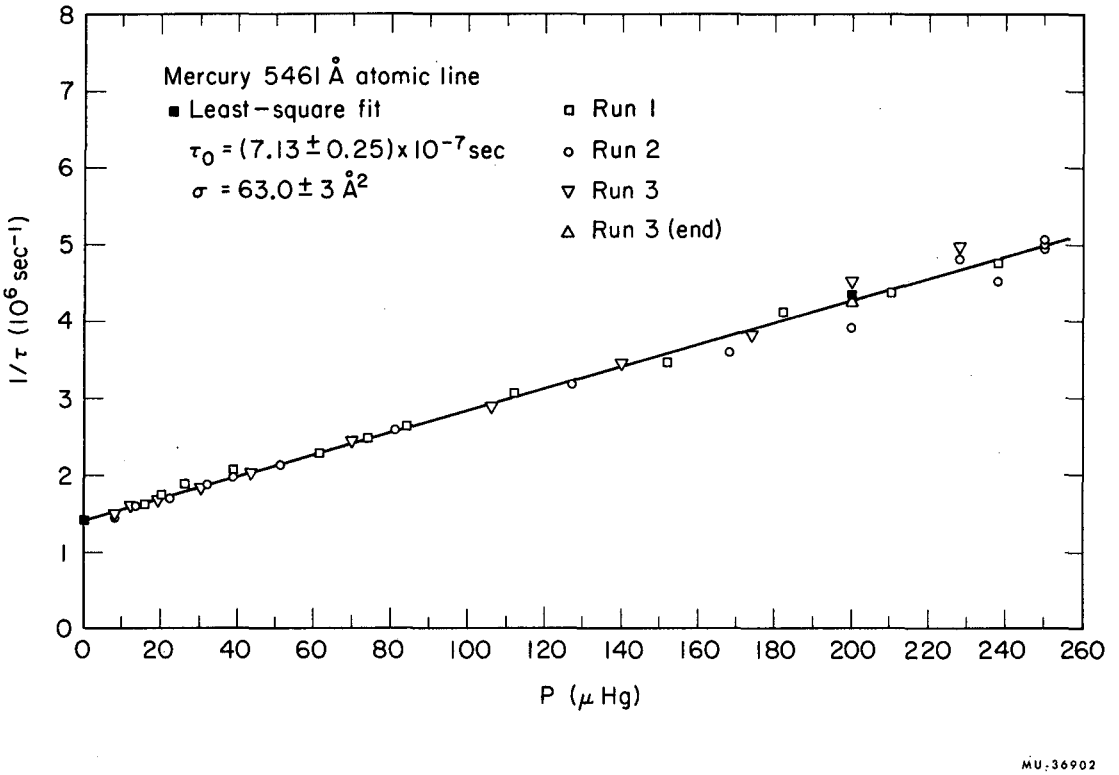
Mercury 5461 Å atomic line
■ Least-square fit
$\tau_0 = (7.13 \pm 0.25) \times 10^{-7}$ sec
$\sigma = 63.0 \pm 3$ Å^2
□ Run 1
○ Run 2
▽ Run 3
△ Run 3 (end)
$1/\tau$ (10^6 sec^{-1})
P (μ Hg)
0
1
2
3
4
5
6
7
8
0
20
40
60
80
100
120
140
160
180
200
220
240
260
MU-36902

Fig. 23

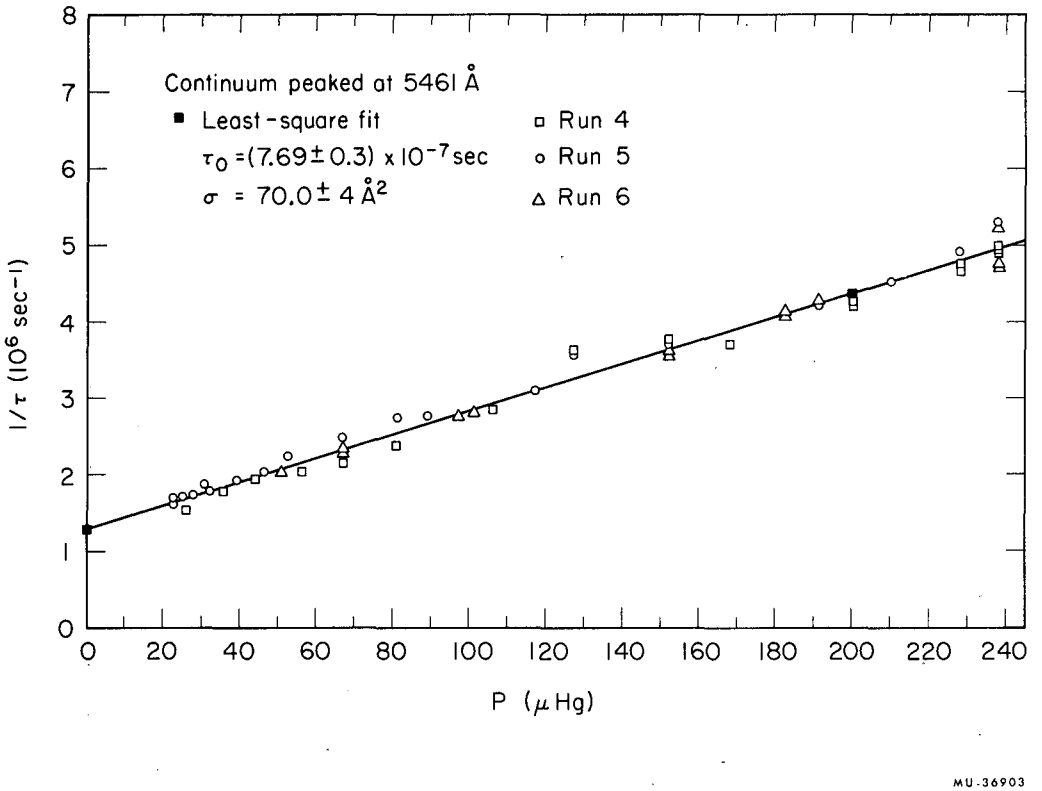
Continuum peaked at 5461 Å
Least-square fit
$\tau_0 = (7.69 \pm 0.3) \times 10^{-7}$ sec
$\sigma = 70.0 \pm 4$ Å^2
Run 4
Run 5
Run 6
$1/\tau$ (10^6 sec^{-1})
P (μ Hg)
0
1
2
3
4
5
6
7
8
0
20
40
60
80
100
120
140
160
180
200
220
240
MU-36903

Fig. 24

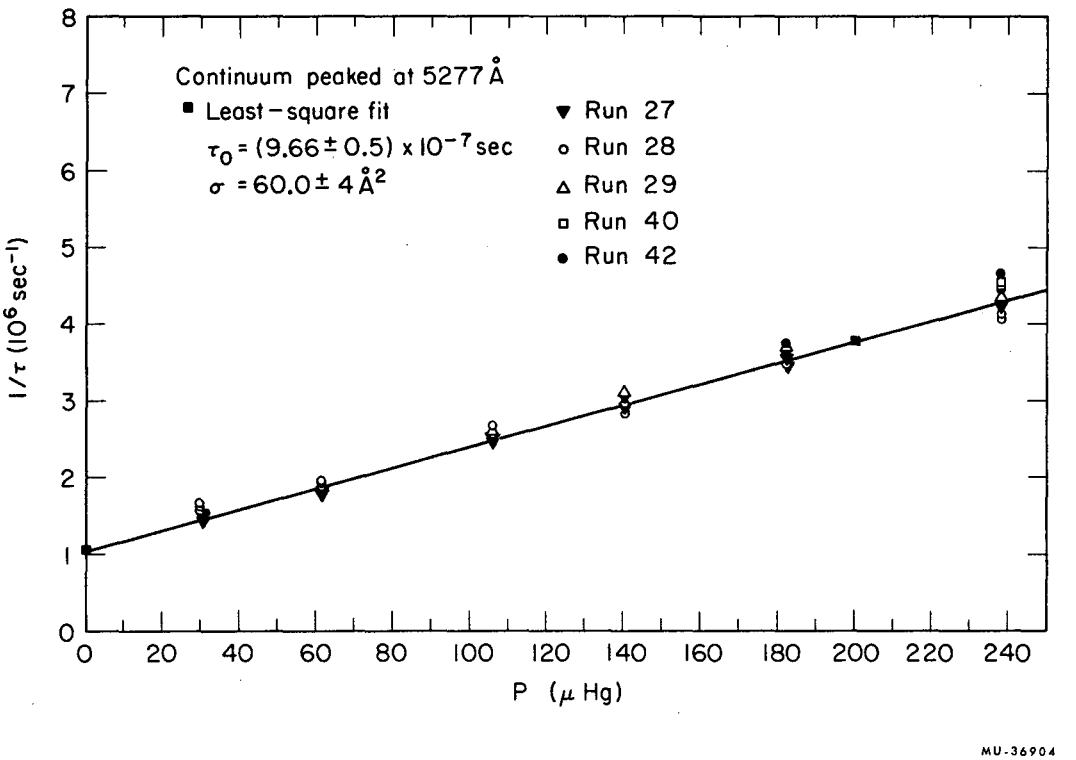
Continuum peaked at 5277 Å
Least-square fit
$\tau_0 = (9.66 \pm 0.5) \times 10^{-7}$ sec
$\sigma = 60.0 \pm 4$ Å^2
Run 27
Run 28
Run 29
Run 40
Run 42
$1/\tau$ (10^6 sec^{-1})
P (μ Hg)
0
1
2
3
4
5
6
7
8
0
20
40
60
80
100
120
140
160
180
200
220
240
MU-36904

Fig. 25

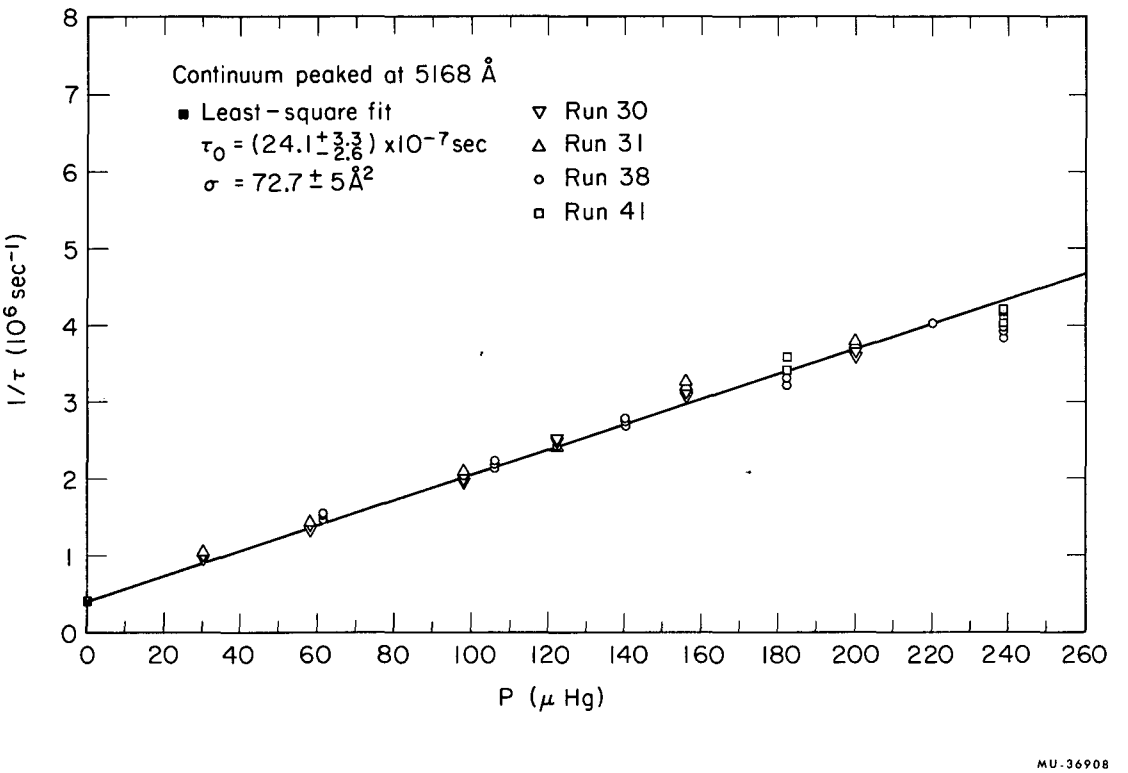
Continuum peaked at 5168 Å
■ Least-square fit
$\tau_0 = (24.1^{+3.3}_{-2.6}) \times 10^{-7}$ sec
$\sigma = 72.7 \pm 5$ Å^2
▽ Run 30
△ Run 31
○ Run 38
□ Run 41
1/τ (10^6 sec^{-1})
P (μ Hg)
0
1
2
3
4
5
6
7
8
0
20
40
60
80
100
120
140
160
180
200
220
240
260
MU-36908

Fig. 26

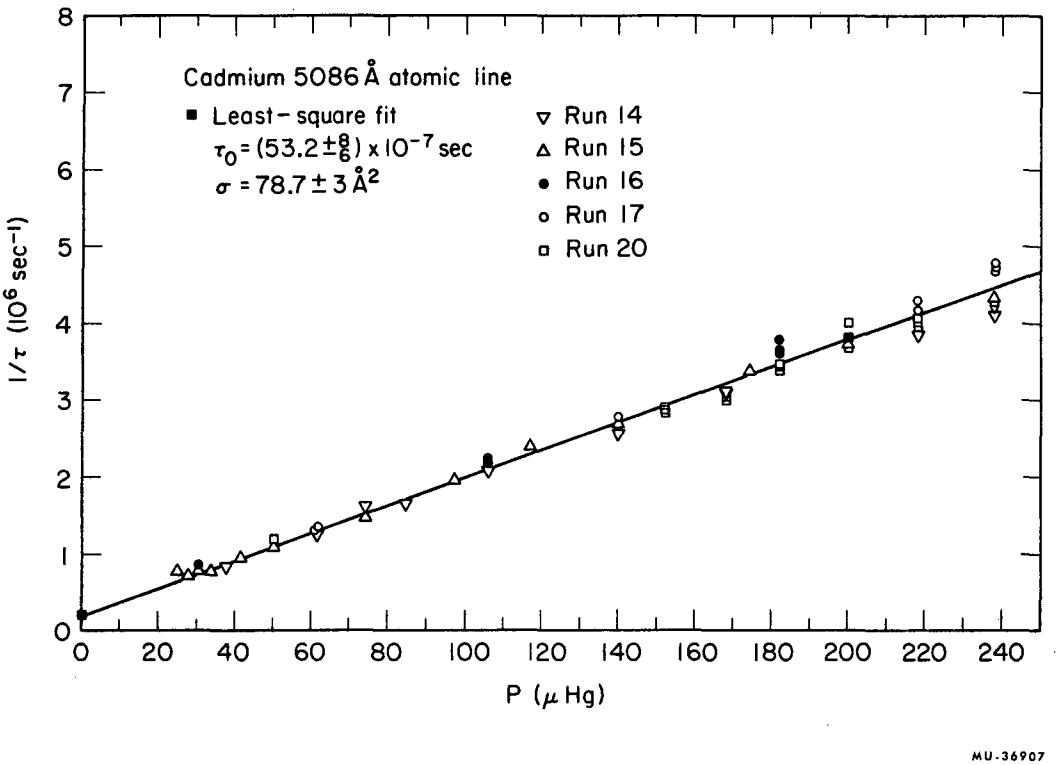
Cadmium 5086 Å atomic line
■ Least-square fit
$\tau_0 = (53.2 \pm \frac{8}{6}) \times 10^{-7}$ sec
$\sigma = 78.7 \pm 3$ Å^2
▽ Run 14
△ Run 15
● Run 16
○ Run 17
□ Run 20
$1/\tau$ (10^6 sec^{-1})
P (μ Hg)
0
1
2
3
4
5
6
7
8
0
20
40
60
80
100
120
140
160
180
200
220
240
MU-36907

Fig. 27

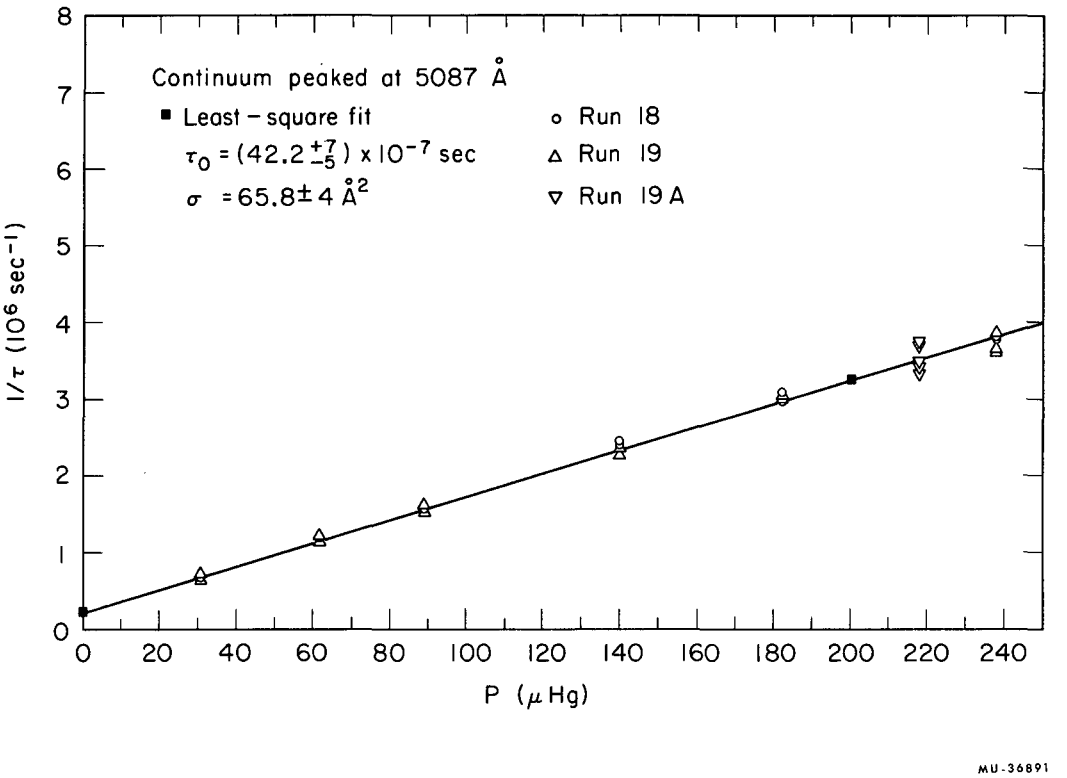
Continuum peaked at 5087 Å
■ Least – square fit
$\tau_0 = (42.2^{+7}_{-5}) \times 10^{-7}$ sec
$\sigma = 65.8 \pm 4$ Å^2
o Run 18
Δ Run 19
▽ Run 19 A
1/τ (10^6 sec^{-1})
P (μ Hg)
0
1
2
3
4
5
6
7
8
0
20
40
60
80
100
120
140
160
180
200
220
240
MU-36891

Fig. 28

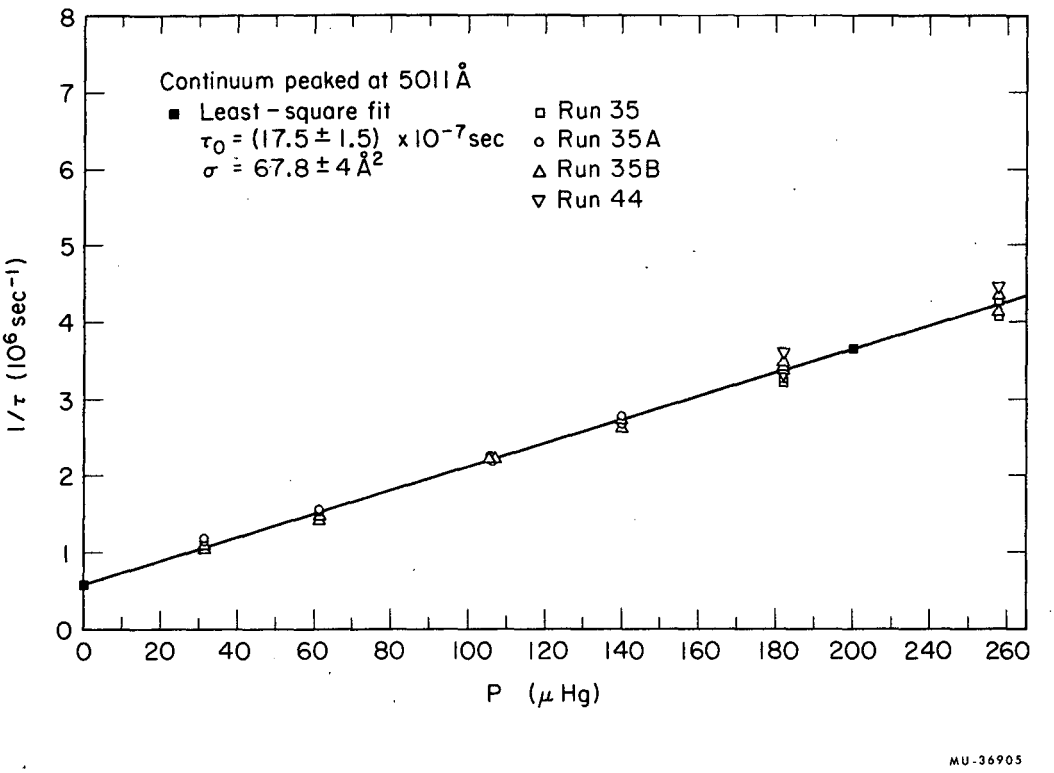
Continuum peaked at 5011 Å
■ Least-square fit
$\tau_0 = (17.5 \pm 1.5) \times 10^{-7}$ sec
$\sigma = 67.8 \pm 4$ Å^2
□ Run 35
○ Run 35A
△ Run 35B
▽ Run 44
1/τ (10^6 sec^{-1})
P (μ Hg)
0
1
2
3
4
5
6
7
8
0
20
40
60
80
100
120
140
160
180
200
240
260
MU-36905

Fig. 29

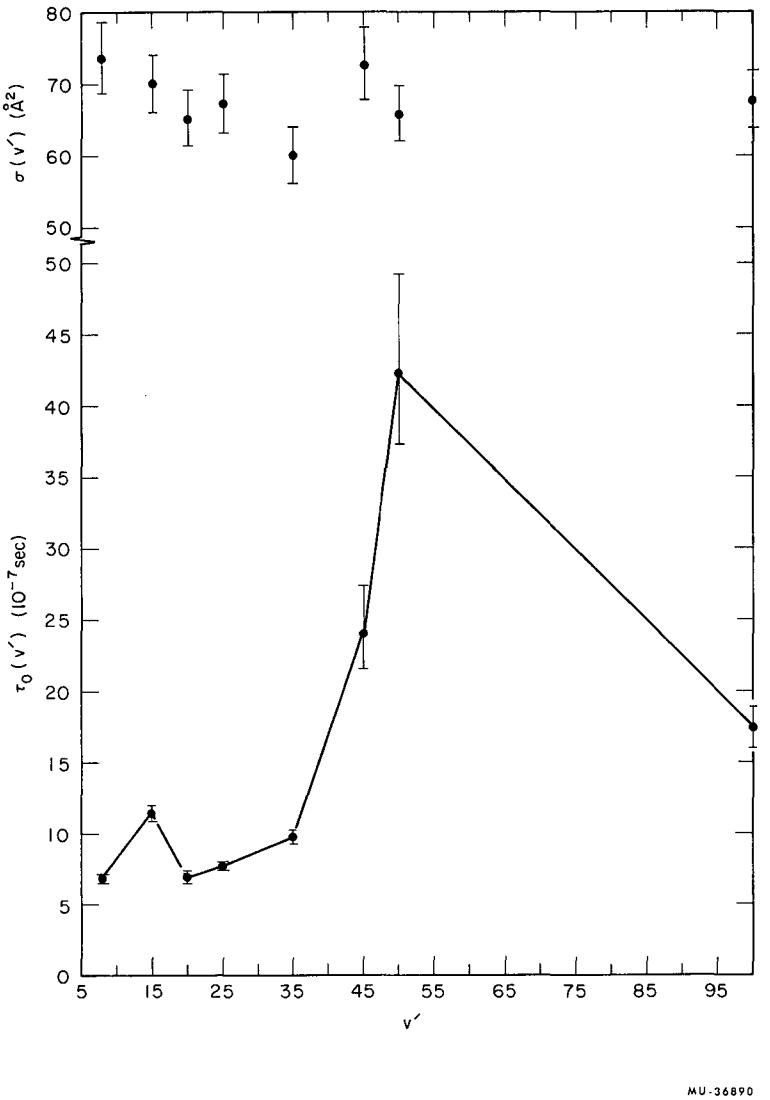
80
70
60
50
50
45
40
35
30
25
20
15
10
5
0
$\sigma(v')$ (Å^2)
$\tau_0(v')$ (10^{-7} sec)
5
15
25
35
45
55
65
75
85
95
v'
MU-36890

Fig. 30

VII. DISCUSSION

A. I_2 Spectroscopic Data

The iodine molecule is one of the most thoroughly investigated molecules known.[43] The potential energy curves for the $X^1\Sigma_{0^+_g}$ and $B^3\Pi_{0^+_u}$ states have been analyzed to very high vibrational levels, the vibrational and rotational constants for these states accurately determined, and the vibrational levels in the B state recently renumbered.[44,45]

The vibrational term values (in cm^{-1}) are given by the usual expansion (ref. 46, p. 92).

$$G(\omega) = \omega_e(v+\tfrac{1}{2}) - \omega_e x_e(v+\tfrac{1}{2})^2 + \omega_e y_e(v+\tfrac{1}{2})^3 + \omega_e z_e(v+\tfrac{1}{2})^4 + \ldots \quad (18)$$

and the rotational terms by

$$B_v = B_e - \alpha_e(v+\tfrac{1}{2}) + \gamma_e(v+\tfrac{1}{2})^2 + \delta_e(v+\tfrac{1}{2})^3 + \ldots. \quad (19)$$

The values of the constants in Eqs. (18) and (19) are given for the X state by Rank,[44] and for the B state by Steinfeld, et al.[45] and are summarized in Table V. The internuclear separation r_e of the upper state is greater by ~ 0.4Å than that of the X state, and its dissociation energy D_e is approximately 4391 cm^{-1}, with an uncertainty in the convergence wavelength at 4990Å of ±5Å.

After determining the new constants for the B state, Steinfeld, et al. found they had to decrease the vibrational numbering of that state by one unit over the original assignment by Mecke and Loomis[47] in order to bring their calculated intensity distributions into agreement with the known fluorescence intensities. This renumbering has been confirmed by Brown and James[48] who compared the observed isotopic shift of a given band origin to the calculated value for various choices of v'.

Table V. Spectroscopic Constants

	$B^3\Pi_{0^+_u}$	$X^1\Sigma_{0^+_g}$
ω_e	125.273 cm^{-1}	214.519 cm^{-1}
$\omega_e x_e$	0.7016	0.60738
$\omega_e y_e$	- 0.00567	- 0.001307
$\omega_e z_e$	3.2×10^{-5}	-5.04×10^{-6}
D_e	4391	12559.6 [a,b]
T_e	15770.59	
B_e	0.028969	0.037389
α_e	1.562×10^{-4}	1.210×10^{-4}
γ_e	-4.00×10^{-7}	1.90×10^{-8} (calc)
δ_e	-3.5×10^{-8}	8.57×10^{-11}
r_e	3.028Å	2.669Å [a]

a Verma[53]

b Zare[49] (Ref. 13)

B. Construction of the B and X State Potential Curves

Zare[49,72] used the Rydberg-Klein-Rees procedure,[50-52] to calculate classical right- and left-hand turning points of the B and X states. With the smoothed potential curve drawn through these points, he solved the radial Schrödinger Equation for the vibrational eigenfunctions $\psi_{v'}$ and $\psi_{v''}$ (where v' and v" refer to the B and X states, respectively) and calculated Franck-Condon factors $q_{v',v''} = \left| \int \psi_{v'}\psi_{v''}\, dr \right|^2$ for v' = 15, 16, and 26 to v" = 0 to 69. He was able to match the known fluorescence intensities with the older vibrational numbering by varying B'_v within the experimental error. The correction with v' = 25 and the more accurate B'_v appears in Ref. (45).

Verma[53] used the same procedure to map the turning points of the X state from v" = 0 to v" = 112 almost at the dissociation limit. He observed the ultraviolet fluorescence spectrum from 1830-2370Å and measured the spacing between the fluorescence P and R doublets up to the convergence limit.

C. The Quenching of I_2 Fluorescence

Because of the many repulsive states originating from the atomic $^2P_{3/2} + {}^2P_{3/2}$ and $^2P_{3/2} + {}^2P_{1/2}$ configurations the iodine molecule in the B state can predissociate; i.e. it can dissociate to two I atoms via a nearby repulsive state, while possessing less energy than the dissociation limit of the B state.

By exciting I_2 vapor in a magnetic field of 12,500 G with narrow band continua and atomic lines, Turner was able to observe the ratio of magnetically quenched to unquenched fluorescence intensity at each wavelength.[54,55] The quenching started at v' ~ 13, peaked at v' ~ 25, and

decreased slowly thereafter.

Turner and Samson[56] observed absorption of the $^2P_{3/2}$ 1830.4Å resonance line from iodine atoms by a tube filled with I_2 (0.3 mm pressure) and argon (50 mm) while the tube was illuminated with wavelengths greater than 5100Å. With no argon present, he observed only feeble absorption of the resonance line, which he attributed to rapid diffusion of the atoms to the walls. Later comparison with the I_2 fluorescence spectrum from a mixture of I_2 (0.3 mm) and argon (11 mm) showed a weakening of the bands for $\lambda > 5710$Å ($v' > 14$).[57] The effect of the argon was to increase the I atom concentration by causing collision-induced predissociation of the I_2 molecules. Loomis and Fuller[58] had earlier measured the fluorescence quenching of I_2 (0.2 mm) by O_2 (few cm to 1 atm). They observed a greater absorption from the continuum at wavelengths corresponding to $v' > 12$. The effect peaked at $v' \sim 25$, similar to Turner's observations, and decreased at shorter wavelengths. It was attributed to a broadening of the absorption lines due to shortening of the lifetimes of the excited vibrational levels by a predissociative crossover.

Van Vleck[59] gives a detailed analysis of the symmetries of electronic states that may mix in the magnetic and collisional quenching cases. The analysis for I_2 is complicated somewhat by the fact that in Hund's case a (Λ,S) coupling does not apply, and only $\Omega = (m_{J_1}, m_{J_2})$ holds in case c.[46] For $\Omega = 0$, the states are grouped into 0^+ and 0^- if the total wavefunction is even or odd on reflection of the orbital and spin coordinates through an internuclear plane, and in the presence of a magnetic field, this reflection symmetry is lost.

The possible molecular states of type $0^{+,-}_{g,u}$ derived from the ground

level $^2P_{3/2} + {}^2P_{3/2}$ atoms are $^3\Sigma_u^+$, $^3\Pi_{0^-u}$ (symmetry 0_u^-) and $^1\Sigma_g^+$, $^3\Pi_{0^+g}(0_g^+)$. For $^2P_{3/2} + {}^2P_{1/2}$ atoms, the states of interest are $^1\Sigma_u^-$, (0_u^-), $^3\Pi_{0^-g}(0_g^-)$ and $^3\Pi_{0^+u}(0_u^+)$, $^3\Sigma_g^-(0_g^+)$. The B $^3\Pi_{0^-u}$ state of I_2 may mix with the following states: $^3\Sigma_u^+$, $^3\Pi_{0^+u}$ from $^2P_{3/2}$ atoms; and $^1\Sigma_u^-$ from the $^2P_{3/2} + {}^2P_{1/2}$ atomic states. The repulsive $^1\Sigma_u^-$ will always lie above the other two 0_u^- states since it originates at a higher energy and can never cross other states of the same symmetry. The $\sigma_g^2 \pi_u^3 \pi_g^3 \sigma_u^2\ ^3\Sigma_u^+$ configuration contains one more anti-bonding electron than the $\sigma_g^2 \pi_u^4 \pi_g^3 \sigma_u\ ^3\Pi_{0^-u}$ configuration, so that its potential curve will rise faster with smaller internuclear distance than that of the $^3\Pi$ state. The order in decreasing energy would then be $^1\Sigma_u^- > {}^3\Sigma_u^+ > {}^3\Pi_{0^-u}$.

There are also states originating from the $^2P_{3/2}$ atomic states which can combine with the B state through an electric dipole term, where the usual selection rules are $g \leftrightarrow u$, $+ \leftrightarrow +$, $- \leftrightarrow -$, $\Delta\Omega = 0, \pm 1$. The spontaneous transition probability of the emitting state can be written as

$$A = \frac{8\pi c}{N_0} \frac{2303}{\langle \lambda_f^3 \rangle} \frac{g''}{g'} \int \epsilon \, d \ell n \, \lambda \qquad (20)$$

where N_0 is Avogadro's number, $\langle \lambda_f^3 \rangle$ the mean of the cubed fluorescent wavelength, ϵ the decadic molar extinction coefficient, and g" and g' the multiplicities of the lower and upper electronic states, respectively. For small separations in energy, the λ_f^3 term would prohibit any transitions, so that strong emission from the B state to some nearby repulsive state would require a large f-value or a short enough λ. These nearby repulsive states could be $^3\Pi_{1g}$ or $^3\Pi_{0^+g}$ ($\Delta\Omega = +1, 0$ respectively).

Kondratjew and Polak[60] observe three extinction maxima in the visible absorption spectrum of I_2 at v' = 22, 29, 39 and assign them

to $^3\Pi_{0^+u} \rightarrow {}^1\Pi_{1u}$, $^3\Pi_{1u}$ and $^3\Pi_{0^+g}$ crossovers. Thus, a whole host of states may contribute to predissociation. In fact, Zener indicates that no special selection rules have to be obeyed in collision-induced predissociations.[61]

D. Self-Quenching Cross Sections

One would expect that the measured quenching cross-sections would show some of the effects of dissociative levels' crossing the B state. The results indicate, however, that they are independent of v', and show no unusual effects at v' ~ 25, or v' = 22, 29, or 39. The lack of variation could be explained if another predissociating state drew near enough to the B state at small internuclear distances to allow mixing, and ran parallel to high v'. A suitable state is the $^3\Pi_{0^-u}$ which would interact via magnetic mixing with the $^3\Pi_{0^+u}$ state.

A comparison of the cross sections obtained by excitation with the Hg 5461Å and Na D wavelengths with the recent work of Brown and Klemperer[62] show fair agreement. Since they used the v' = 25 lifetime of $(7.2\pm1)\times10^{-7}$ sec obtained by Brewer, et al.[63] to obtain quenching cross sections from their Stern-Volmer quenching plots, their reported values should be multiplied by a factor of 7.2/7.13 for the mercury line excitation, and 7.2/11.9 for the Na D line excitation (see their Table VI). Their results after correction are 91.1 ± 2.4Å^2 and 78.7 ± 5.3Å^2, as compared with our values of 63.0 ± 3Å^2 and 69.4 ± 3Å^2 for the mercury and sodium wavelengths, respectively. The value of 63.0Å^2 is also in excellent agreement with the value of 67.5Å^2 from the quenching measurements of Arnot and McDowell.[64] A possible error in Brown and Klemperer's measurements would arise if the finger temperature of their resonance cell did not control the I_2 vapor pressure.

E. Kinetics of I_2 Dissociation and Recombination

The decay of excited I_2 molecules is the result of competition by a radiative decay, a spontaneous predissociative decay, and a decay through collision-induced predissociation (self-quenching). The first two rates are dependent only on (I_2^*) (the concentration of excited I_2) whereas the last depends on the proximity of other I_2, or foreign gas, molecules.

In the presence of 200-500 torr of He, Ne, A and N_2, Rabinowitch and Wood[65] found that if they assumed a quantum yield $\gamma = 1$ for the process $I_2^* + X \rightarrow I + I + X$ for excitation with light on the short wavelength side of the convergence limit, then γ was equal to unity for band regions in the long wavelength region. So that at high pressures of quenching gas, all I_2^* molecules dissociate into atoms by collisions with the quenching gas molecules. At low pressures, they assert that the major process is the natural decay $I_2^* \rightarrow I_2 + h\nu$, and that the quantum yield of atom production is $\gamma = 1$ above 4990Å, and $\gamma = 0$ below.[66] No experimental data is given for the quantum yields in the low pressure region.

An important piece of evidence for the production of atoms stems from the measurement of paramagnetic absorption of I atoms by dissociation of I_2 vapor in a resonator cavity. Bowers, et al.[67] irradiated I_2 at pressured below 1 torr with wavelengths above and below the dissociation limit, and observed the resonance absorption of atoms with changes in I_2 pressure, exciting wavelength, magnetic field, and addition of air. They found no change in I atom concentration with changes in I_2 partial pressure between 0.02 and 0.2 mm, and no change with the addition of air and I_2 partial pressure held fixed at 0.1 mm. These results were independent of wavelength for λ greater or less than 4900Å. They also noted

no change in the atom absorption with a factor of 2 change in the magnetic field.

It is difficult to reconcile these observations with the know reactions of I_2. All possible fates of I_2^* and I may be shown through the following reactions:

absorption	$I_2 + h\nu \xrightarrow{\alpha I_o} I_2^*$	(21)
spontaneous emission	$I_2^* \xrightarrow{1/\tau_o} I_2 + h\nu$	(22)
spontaneous predissociation	$I_2^* \xrightarrow{k_P} I + I$	(23)
self-quenching	$I_2 + I_2^* \xrightarrow{k_Q} I + I + I_2$	(24)
gaseous recombination	$I + I + I_2 \xrightarrow{k_R} I_2 + I_2$	(25)
wall recombination	$2I \xrightarrow{k_W} I_2\ (W)$	(26)

The rate constant for absorption is αI_0, with I_0 the incident light intensity, and α the fraction of light absorbed. The rate $1/\tau_0$ is the purely radiative rate of I_2^* decay at zero I_2 pressure.

If in the steady-state approximation we write

$$\frac{d(I_2^*)}{dt} = \alpha I_0(I_2) - \frac{1}{\tau_0}(I_2^*) - k_Q (I_2)(I_2^*) - k_P (I_2^*) = 0$$

$$\frac{d(I)}{dt} = k_Q (I_2)(I_2^*) + k_P (I_2^*) - k_R (I)^2 (I_2) - k_W (I)^2 = 0$$

then

$$(I)^2 = \alpha I_0 (I_2) \frac{k_P + k_Q (I_2)}{k_W + k_R (I_2)} \frac{1}{(\frac{1}{\tau_0} + k_P) + k_Q (I_2)} \quad (27)$$

At high I_2 pressures where k_P and k_W are small relative to $k_Q(I_2)$

$$(I)^2 = \alpha I_0 \frac{k_Q}{k_R} \cdot \frac{1}{(\frac{1}{\tau_0} + k_P) + k_Q(I_2)} (I_2) \quad (28)$$

And at very high pressures where the quantum yield of quenching is substantially greater than that of fluorescence,

$$(I)^2 = \alpha I_0/k_R \quad (29)$$

which is independent of (I_2).

Finally at low pressures, where the quantum yield of fluorescence is close to unity,

$$(I)^2 = \alpha I_0 \frac{k_P}{k_W} \frac{1}{\frac{1}{\tau_0} + k_P} (I_2). \quad (30)$$

If a magnetic field and foreign gas quenchers are present, new terms of k_M, $k'_Q(X)$, and $k'_R(X)$ will have to be added to the numerator and denominator of Eq. (27). Here, k_M is the rate constant for magnetic quenching, and the primes indicate the new rate constants with foreign gas X. If the magnetic field is large, k_M will dominate and the final result will again reduce to Eq. (29). From Fig. 23, we find that over the pressure range studied by Bowers, et al., $0.21 < k_Q(I_2)/1/\tau_0 < 2.04$; i.e., the collisional quenching and the natural decay rates are comparable. In order to be in the range of Eq. (29) the ratio $k_Q(I_2)/1/\tau_0$ would have to be > 10, which

occurs at pressures of $I_2 > 0.98$ mm ($T > 39°C$). It appears, then, that Bowers was working with magnetic fields where the magnetic, rather than collisional, quenching predominated, and where (I) is given by Eq. (29).

To get some idea of the magnitude of k_w as a function of particle density, we note that in a time Δt the iodine atom will have moved a distance Δx through the vapor with diffusion coefficient D, where $(\Delta x)^2 = 2D\Delta t$. The diffusion coefficient can be expressed as[68]

$$D = \frac{3\pi}{32}\left(\frac{1}{\pi N_t \sigma_{12}^2}\right)\left(\frac{8kT}{\pi\mu}\right)^{1/2}$$

where N_t = total number of I_2 molecules, $\sigma_{12} = 1/2(\sigma_I + \sigma_{I_2}) = 1/2(4+8) = 6\text{Å}$, and μ is the reduced mass of I and I_2. For $T = 273°K$ and an I_2 pressure of 0.03 mm, $N_t = 1.07\text{X}10^{15}$/cc, with a mean free path of 0.39 mm, an average velocity of $2.62\text{X}10^4$ cm/sec, and $D = 639$ cm^2/sec. For a cell radius of 2 cm, $\Delta t = 2/639 = 3.13\text{X}10^{-3}$ sec. In this diffusion time, an iodine atom will suffer approximately $\bar{Z}\,\Delta t = 6.45\text{X}10^4\, N_t \sigma_{12}^2\, (T/\mu)^{1/2}\, \Delta t$ collisions, where $\bar{Z}$ is the average number of $I\text{-}I_2$ collisions/sec. Using $N_t = 10^{15}$/cc, $\sigma_{12} = 6\text{Å}$, and $T = 273°K$, this is about $2\text{X}10^3$ collisions. Assuming an iodine atom-to-molecule ratio of 10^{-3}, the iodine atom will make only 10^{-3} times as many collisions with other I atoms at these pressures; i.e., it will have diffused to the walls, and the recombination will be heterogeneous. As the I_2 pressure increases, the total number of I-I collisions will increase as the square of the I_2 pressure, so that the recombination will quickly become homogeneous. At an I_2 pressure of 0.1 mm, the I-I collisions will have increased by a factor of 10 to ~20 collisions in a diffusion time of 10^{-2} sec.

Since Bowers used a cell of radius 0.7 cm, he should certainly have been in the region governed by Eq. (30), so that his observations would warrant repeating. Also, it still is not certain from Bower's measurements or from the previous work by Turner and others whether or not iodine atoms are produced in T_2-I_2 collisions in the absence of external magnetic fields.

F. Radiative Lifetimes

The resonance spectra excited by low to medium pressure light sources have been studied by Dymond[69,55] and recently by Brown and Klemperer.[62] For a narrow Hg 5461Å line, the excited level is v' = 25, J' = 34; for the Na D (reversed) lines, v' = 14, J' = 113 (10%); v' = 15, J' = 44 (75%); and v' = 16, J' = 106 (10%); and for the Cd 5086Å line, v' = 49, J' = 8; v' = 50, J' = 43. The assignment of the other levels in Table IV was made using Eq. (18) and the data in Table V. The 5011Å assignment is only an estimate, taking into account the fact that the vibrational spacing is extremely small near the dissociation limit.

From Table IV we see that no great differences in either cross section or lifetime were observed when excitation was made with either an atomic line, or a narrow spread of wavelengths peaked at the atomic line wavelength. Since iodine has many absorption lines in the region of each continuum excitation, the results indicate that the lifetime is independent of v' over a small interval ($\Delta v' \sim 2$-3) of levels. In terms of the Franck-Condon overlap, the lifetime of state v' can be expressed as

$$\frac{1}{\tau_{v'}} = \frac{64\pi^4}{3h} g'' \cdot \bar{R}_e^2 \sum_{v''} \nu_{v'v''}^3 \, q_{v'v''} \qquad (31)$$

where g" is the degeneracy of the lower electronic state, $\nu_{v'v''}$ the fluorescent frequency, $q_{v'v''}$ the overlap between levels v' and v", and $\bar{R}_e$ an average value of the electronic contribution to the transition moment evaluated at the r-centroid[70] of the transition. The present results imply that the sum changes only slightly from v' = 25 (narrow line excitation) to 24,25,26 (continuum excitation). This is reasonable since the differences between the 24,25 and 26 node wavefunctions is small, and the major influence on $q_{v'v''}$ will be the position of the nodes in the lower state. Experimentally, Polanyi observes this when he notes that the doublet intensities of the series 25'-0", 1"...; 26'-0", 1"...; 27'-0", 1"..., are nearly the same.[71]

Zare's compiled RKR program[72] can, in principle, be extended to calculate Franck-Condon overlap integrals to high v' ~ 100. However, on the basis of Franck-Condon factors alone, one would predict smooth changes in the overlaps and intensity sums from level to level, and would find it difficult to account for the peaks at v' = 15 and 50, and the rapid decrease after v' = 50. Either of two processes could compete with the B → X fluorescence and lower the lifetimes of the high v' levels. The $^1\Pi_u$ state mixing with the B state near v' = 100 could cause spontaneous predissociation, in which the measured lifetime would be $1/\tau_0 + k_p$. And the $^3\Pi_{1g}$ could be a possible state to which a dipole transition could occur ($\Delta S = 0$, $u \leftrightarrow g$) with the radiation emitted in the infra-red.

G. Lifetime and Absorption

If an absolute transition probability A(v',J';v",J") of a given line is measured, together with the relative intensities of fluorescence I(v',v") in quanta/second, then the lifetime of the emitting state is

$$\tau_{v'} = \frac{I(v',v'')}{A(v',J';v'',J'')\Sigma_{,v''}I(v',v'')} \qquad (32)$$

The relative intensities were calculated from the Franck-Condon factors of Steinfeld[73] using the relation $I(v',v'') = \nu^3_{v',v''}\, q_{v',v''}$ with I in quanta (transitions)/second. The range of levels was 14' - 0"... 55"; 15' - 0"... 55"; 25' - 0"...67", and represented all the members of the fluorescence series with non-zero overlaps. The lifetimes obtained in the present work were used in Eq. (32) to compute A(v',J'; v",J") which was compared with the values of Brown and Klemperer. The values obtained appear in column 3 of Table VI and the measured values in column 2.

The Einstein absorption coefficients, B, were caluclated from the absorption data of Rabinowitch and Wood,[74] and from Sulzer and Wieland,[75] and compared with the B values from column 2. The relationship between B and the integrated absorption curve is

$$B = \frac{2303}{N_0}\frac{4\pi}{h}\int \epsilon\, d\, \ell n\, \lambda = 7.252X10^6 \int \epsilon\, d\, \ell n\, \lambda \text{ cm}^2\text{erg}^{-1}\text{sec}^{-1}$$

where N_0 is Avogadro's number, h Planck's constant, and the units of radiation those for isotropic intensity (intensity per sq. cm. normal to the light). The relation between A and B in these units is $B = A/2ch\nu^3$ with c the speed of light and ν the frequency of the transition in cm^{-1}.

The Einstein B coefficient can also be related to the transition moment matrix element. Assuming the validity of the rigid rotator-harmonic oscillator sum rules, the final result becomes[46]

$$B = \frac{32\pi^4}{3h^2c}\,|R_e|^2$$

where $|R_e|$(erg cm^3) is the absolute value of the electronic contribution to the total transition moment. Thus, B should be a constant for a given electronic transition insofar as $|R_e|^2$ is constant.

The lifetimes and the single line absorption measurements can all be compared with the total band absorption measurements on the basis of the B values. The quantity $B_{a'}$, may be defined as the sum of absorption coefficients from all v" levels in the X state to an a' level in the upper state, and is given in terms of the calculated overlaps as

$$B_{a'} = \sum_{v''} B_{a'v''} = B_{a'b''} \frac{\sum_{v''} q_{a'v''}}{q_{a'b''}} \qquad (33)$$

where R_e is assumed to be constant.

If we assume the sum rule to hold for progressions in v', then we can write $\sum_{v'} q_{v'b''} = \sum_{v''} q_{a'v''} = 1$, where the last equality follows from the tabulated overlaps. We then see from Eq. (33) that $B_{b''} = \sum_{v'} B_{v'b''} = B_{a'}$ where $B_{b''}$ is the total absorption from any b" level to <u>all</u> v' levels.

The $B_{a'}$ can be derived also from the lifetime measurements and the mean fluorescent frequency by combining Eqs. (32) and (33) to give

$$B_{a'} = \frac{\sum_{v''} q_{a'v''}}{\sum_{v''} \nu_{a'v''}^3 q_{a'v''}} \left(\frac{1}{2hc}\right)\left(\frac{1}{\tau_{a'}}\right) \qquad (34)$$

The sum in the denominator is the mean of the cubed fluorescent frequency, and is known for a' = 14 (8350Å), 15 (8380Å), and 25 (8760Å).

The total band absorptions of Rabinowitch and Wood, and Sulzer and Wieland are really sums of $B_{b''}$ for b" = 0, 1, 2, ..., each weighted by its Boltzmann factor. In the approximation $\sum_{v'} q_{v'b''} = 1$, $B_{0''} = B_{1''} = B_{2''}$....so that <u>any</u> of the $B_{b''}$ may be compared with the $B_{a'}$, derived from the lifetimes and the mean cubed fluorescent frequency.

Table VI. Measured and Calculated Transition Probabilities for I_2

Line	$A(10^5/sec)$	$A(10^5/sec)$ (calc. from Eq.(32)	$\int \epsilon d\ell n\lambda$	$B_{a',b''}(10^8 cm^2/erg\ sec)$ (from col.3)	$B(10^8 cm^2/erg\ sec)$ [$B_{a'}$ from Eq.(34) or $B_{b''}$ from col.4]
14-3 P(114)	3.1±0.3[a]	0.75±0.08		0.40±0.04	12.3±0.6
15-3 P(45)	1.20±0.25[a]	0.57±0.06		0.33±0.03	12.4±0.6
25-0 R(33)	>> 0.14[b]	1.53±0.15		0.63±0.06	23.6±1.3
			155±30[c]		9.71±1.9
			134±20[d]		11.3±2.2

a Reference 62.

b Reference 29

c References 49 and 74.

d References 49 and 75.

The $B_{a'}$ values for a' = 14, 15 and 25 are given in Table VI, column 6, along with the total band measurements from column 4. The results for all the a' levels for which lifetimes were measured are shown in Fig. 31. The horizontal solid lines indicate the total band absorption values, and the dotted lines the spread in their values. The mean fluorescent wavelengths were not known for each a', and were estimated to ± 10% by noting the trend in the three known wavelengths, and the value of 8890Å at v' = 27. The values used were 7950Å (8'), 8550Å (20'), 9150Å (35'), 9380Å (45'), 9470Å (50'), and 9710Å (100').

The results show that the wavelength effect is insufficient to make the $B_{a'}$ agree with the total band absorptions. In fact, since the mean fluorescent frequency decreases with increasing v', the effect on the basis of the lifetimes would be to modify the peak in the lifetime at v' = 50, only to accentuate the peak at v' = 15, as can be seen from Eq. (31). The variation in the $B_{a'}$ indicates that the constancy of R_e and the sum-rule assumptions are not valid in Eq. (34). A more complicated analysis would have to be made in which R_e would be included in the total transition moment rather than removed as an average.

The values of Brown and Klemperer calculated from Eq. (33) are higher than the lifetime B-values as well as those from the total band absorptions. If the sum $A_{14'v''}$ (v'' = 0 to 9) is calculated from their data (ref. 62, Table V) an upper limit to τ_0 is 7.46×10^{-7} sec, which is already smaller than the measured 11.9×10^{-7} sec. Part of the discrepancy is very probably due to overlaps of the 14 - 3 with other more intense lines from the v'' = 1 and 2 absorption series.[76]

The other part may be due to a difference in meaning of columns 2 and 3. The quantity τ_0 is the lifetime extrapolated to zero I_2 pressure where

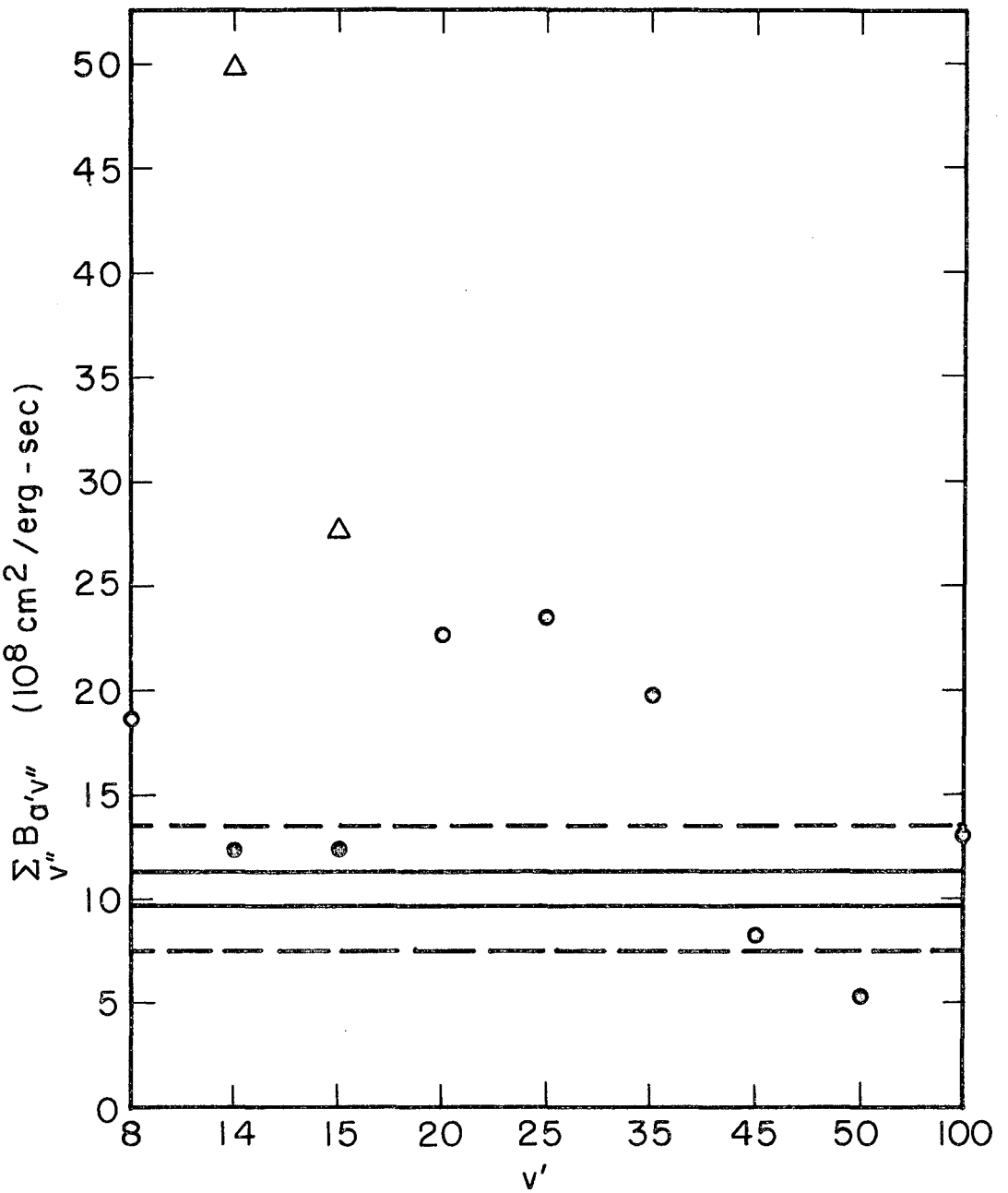
50
45
40
35
30
25
20
15
10
5
0
$\Sigma B_{v'v''}$ (10^8 cm^2/erg-sec)
8
14
15
20
25
35
45
50
100
v'
MUB-9170

Fig. 31

the quenching process does not contribute to the decay of the excited state. A comparison with our $\tau(2.36X10^{-7}$sec) at the 22°C operating temperature of Brown and Klemperer gives for the 14-3 and 15-3 A values in column 3 $(2.27\pm0.23)\times10^{-7}$and 1.72 ± 0.17 respectively, which are in better agreement. Such pressure-dependent absorptions have been observed in I_2 at 2700Å [43] believed to be due to absorption to the $^3\Sigma_u^+$ repulsive state. Whether such an effect were present in the visible band system could be determined by measuring the absorbance at different I_2 path lengths, changing the pressure so as to keep the total number of molecules in the light path constant. No such variation of absorption coefficient with pressure was seen in Brown and Klemperer's data over the pressure range 199-283 μHg for the 14-3 absorption, and 184-235 μHg for the 15-3 line.

Recent absorption and emission measurements on bromine vapor have revealed the presence of both a collision-dependent absorption, and evidence for Br atom's recombining via crossovers from states which mix with the $^3\Pi_{0+u}$ state. Ogryzlo and Sanctuary[77] have measured the absorbance of Br_2 vapor in the region 1850-2500Å at temperatures from 14°C to 300°C using a fixed amount of bromine vapor. The rapid disappearance of a peak at 2080Å with increasing temperatures was ascribed to the breaking of Br_2-Br_2 pairs responsible for the absorption. Using their enthalpy of formation of ΔH_2 = -2.6 kcal, and assuming an entropy of formation of -20 eu, the concentration of the pairs at 30°C is $3X10^{15}$/cc. Integration of their absorption curve at 30°C gives an f-value for the transition of f~0.3.

Gibbs and Ogryzlo[78] studied the orange-red emission ($B^3\Pi_{0+u}$ - $X^1\Sigma_g^+$) from the recombination of Br atoms, and observed a light emission intensity $I \propto (Br)^2(Br_2)$. They cite several mechanisms of recombination consistent with the observed rate law which involve crossovers between

the repulsive $^1\Pi_{1u}$ and weakly attractive $^3\Pi_{0-u}$ state with the $B^3\Pi_{0+u}$ state.

Possible future extension of the work by Bowers, et al., on the EPR absorption of I atoms would help determine the kinetics of I_2 dissociation and I atom recombination. It still has not been conclusively shown, for instance, whether iodine atoms are produced by I_2-I_2 collisions without the presence of a magnetic field.

The measurement of quantum yields of fluorescence and iodine atom formation would be interesting. Alentsev[79] showed that the relative quantum yield of fluoresence in I_2 did not change with exciting wavelengths of 5300Å to 6000Å. However, his measured yield decreased in the important region $\lambda < 5300$Å due to transmission by his monochromator of wavelengths below the dissociation limit of the B state and the subsequent production of I atoms. A measurement of the relative quantum yield in this region would show, for example, whether other transitions were occurring at high v' excitations to account for the decrease in lifetime between v' = 50 and 100.

CONCLUSIONS

No explanation can be given at the present time for the variation of lifetime with vibrational level. Possible spontaneous predissociation or a dipole transition to repulsive states crossing the B state at high v' would account for the decrease of τ_0 between v' = 50 and 100. However, the exact location of these states is not yet known.

The iodine self-quenching cross sections show no variation with vibrational level, especially at v' = 25 where a state of 0_u^- symmetry was presumed to cross. Although our v' = 15 cross section agrees with that of Brown and Klemperer, their v' = 25 value is 30% higher than our value of 63.0$\mathring{A}^2$ and the value of 67.5$\mathring{A}^2$ or Arnot and McDowell. A possible error in their Stern-Volmer measurements would arise if the vapor density in their fluorescence cell was not controlled by the measured temperatures.

A comparison of the I_2-I_2 quenching rates obtained in the present work with a study of the kinetics of iodine atom recombination via EPR absorption shows that the EPR measurements were made in a region where the square of the atom concentration should have been proportional to the I_2 pressure, contrary to the reported results. The discrepancy may arise from the fact that the EPR measurements of Bowers, et al. were made in a region where magnetic, and not collisional, quenching predominated.

The iodine absorption measurements of Brown and Klemperer give total band B-values that are higher than the band absorption measurements of Rabinowitch and Wood, and Sulzer and Wieland; and the B-values obtained from the lifetimes of this work and the Franck-Condon factors of Steinfeld. There is very probable overlap of their 14-3 and 15-3 fluorescence lines with other more intense lines from the v" = 1 and 2 absorption series.

The variation of the lifetime B-values with v' cannot be accounted for by merely a wavelength effect, and indicates that the electronic contribution to the transition moment is changing with vibrational stretching. There is good agreement of the lifetime B-values with the experimental total band absorption values.

REFERENCES

1. E. W. Foster, The Measurement of Oscillator Strengths in Atomic Spectra, Reports on Progress in Physics, p. 469 (1963).

2. John M. Stone, Radiation and Optics, (McGraw-Hill Co., New York, 1963, p. 451).

3. A. C. G. Mitchell and M. W. Zemansky, Resonance Radiation and Excited Atoms, (Cambridge University Press, Cambridge, 1961).

4. G. Stephenson, Proc. Phys. Soc., London, A64, 458 (1951).

5. M. Weingeroff, Z. Physik, 67, 679 (1931).

6. G. M. Lawrence, J. K. Link, and R. B. King, Astrophys. J., 141, 293 (1965).

7. D. Rozhdestvenskii, Ann. Phys. Lpz., 39, 307 (1912).

8. Optical Transition Probabilities, A Collection of Russian Articles 1924-1960 (Israel Program for Scientific Foundations, 1962). Available from the Office of Technical Services, U. S. Dept. of Commerce, Washington 25, D. C.

9. Optical Transition Probabilities, A Collection of Russian Articles 1932-1962, Ibid.

10. N. P. Penkin, J. Quant. Spec. Rad. Transfer, 4, 41 (1964).

11. Yu. I. Ostrovskii, Optika i Spektroskopiya, 2, 673 (1957).

12. S. Heron, R. W. P. McWhirter and E. H. Rhoderick, Nature, 174, 564 (1954).

13. E. Branner, F. R. Hunt, R. H. Adlington and R. W. Nicholls, Nature, 175, 810 (1955).

14. R. G. Bennett, Rev. Sci. Instr., 31, 1275 (1960).

15. O. J. Steingraber and I. B. Berlman, Rev. Sci. Instr., 34, 524 (1963).

16. Jean Brossel and Francis Bitter, Phys. Rev., 86, 308 (1952).

17. A. Lurio and R. Novick, Phys. Rev., 134, A608 (1964).

18. F. W. Byron, Jr., M. N. McDermott, and R. Novick, Phys. Rev., 134, A615 (1964).

19. F. D. Colegrove, P. A. Franken, R. R. Lewis, and R. H. Sands, Phys. Rev. Letters, 3, 420 (1959).

20. P. A. Franken, Phys. Rev., 121, 508 (1961).

21. B. P. Kibble and G. W. Series, Proc. Phys. Soc.,(London), 78, 70 (1961).

22. M. E. Rose and R. L. Carovillano, Phys. Rev., 122, 1185 (1961).

23. P. Thaddeus and R. Novick, Phys. Rev., 126, 1774 (1962).

24. Quicksilver Products, Inc., San Francisco, California.

25. W. Demtröder, Z. Physik, 166, 42 (1962).

26. E. Hulpke, R. Paul and W. Paul, Z. Physik, 177, 257 (1964).

27. G. M. Lawrence, J. Quant. Spec. Rad. Transfer, 5, 359 (1965).

28. G. E. Eng. Bulletin ET-B28,"The Gated Beam Tube and Its Application in Intercarrier T. V."

29. F. E. Stafford, Measurement of Radiative Lifetimes, (Ph. D. Thesis), Lawrence Radiation Laboratory Report UCRL-8854, June 1960.

30. Robert Berg, The Measurement of Radiative Lifetimes, (Ph. D. Thesis), Lawrence Radiation Laboratory Report UCRL-9954, January 1963.

31. M. Kasha, J. Opt. Soc. Am., 38, 929 (1945).

32. Counting Handbook, University of California, Berkeley, Lawrence Radiation Laboratory Report UCRL-3307 (Rev.).

33. P. H. Garrett and H. W. Webb, Phys. Rev., 37, 1686 (1931).

34. W. Zehden and M. W. Zemansky, Z. Physik, 72, 442 (1931).

35. A. Lurio, Bulletin of the Am. Phys. Soc., Series II, 10 (1),49 (1965).

36. H. Kopfermann and Günter Wessel, Z. Physik, 130 100 (1951).

37. Landolt-Bornstein, Zahlenwerte u. Funktionen, (Springer Verlag, Berlin, Germany, 1952), I. Band, 5. Teil, p. 53.

38. R. H. Busey and W. F. Giauque, J. Am. Chem. Soc., 75, 806 (1953).

39. W. T. Hicks, J. Chem. Phys., 38, 1873 (1963).

40. Variable Bandpass Interference Filter Set (No. 60), Optics Technology, Inc., 248 Harbor Boulevard, Belmont, California.

41. S. Glasstone, Textbook of Physical Chemistry, 2nd ed., (D. Van Nostrand Company, Inc., Princeton, N. J., 1946), p. 277.

42. D. A. Shirley and W. F. Giauque, J. Am. Chem. Soc., 81, 4778 (1959).

43. Lois Mathesen and A. L. G. Rees, J. Chem. Phys., 25, 753 (1956).

44. D. H. Rank and B. S. Rao, J. Mol. Spectry., 13, 34 (1964).

45. J. I. Steinfeld, R. N. Zare, L. Jones, M. Lesk, and W. Klemperer, J. Chem. Phys., 42, 25 (1965).

46. G. Herzberg, Spectra of Diatomic Molecules, (D. Van Nostrand, Company, Inc., Princeton, N. J., 1950).

47. F. W. Loomis, Phys. Rev., 29, 112 (1927).

48. R. L. Brown and T. C. James, J. Chem. Phys., 42, 33 (1965).

49. R. N. Zare, J. Chem. Phys., 40, 1934 (1964).

50. R. Rydberg, Z. Physik, 73, 376 (1931).

51. O. Klein, Z. Physik, 76, 226 (1932).

52. A. L. G. Rees, Proc. Roy. Soc., 59, 998 (1947).

53. R. D. Verma, J. Chem. Phys., 32, 738 (1960).

54. L. A. Turner, Z. Physik, 65, 464 (1930).

55. P. Pringsheim, Fluorescence and Phosphorescence (Interscience Publishers, Inc., New York, 1949), p. 200.

56. L. A. Turner and E. W. Samson, Phys. Rev., 37, 1684 (1931).

57. L. A. Turner, Phys. Rev., 41, 627 (1932).

58. F. W. Loomis and H. Q. Fuller, Phys. Rev., 39, 180 (1932).

59. J. H. Van Vleck, Phys. Rev., 40, 544 (1932).

60. E. Kondratjew and L. Polak, Physik Z. Sowjetunion, 4, 764 (1933).

61. C. Zener, Proc. Roy. Soc., 140, 660 (1933).

62. R. L. Brown and W. Klemperer, J. Chem. Phys., 41, 3072 (1964).

63. L. Brewer, R. A. Berg, G. Rosenblatt, J. Chem. Phys., 38, 1381 (1963).

64. C. Arnot and C. A. McDowell, Can. J. Chem., 36, 1322 (1958).

65. E. Rabinowitch and W. C. Wood, J. Chem. Phys., 4, 358 (1936).

66. E. Rabinowitch and W. C. Wood, Trans. Faraday Soc., 32, 553 (1936).

67. K. D. Bowers, R. A. Kamper, and C. D. Lustig, Proc. Phys. Soc., B70, 1176 (1957).

68. S. W. Benson, The Foundation of Chemical Kinetics (McGraw-Hill Book Co., Inc., New York, 1960), p. 184.

69. E. G. Dymond, Z. Physik, 34, 553 (1925).

70. R. W. Nicholls and W. R. Jarmain, Proc. Phys. Soc., 69A, 253 (1956).

71. J. C. Polanyi, Can. J. Chem., 36, 121 (1958).

72. R. N. Zare, Programs for Calculating Relative Intensities in the Vibrational Structure of Electronic Band Systems, University of California Lawrence Radiation Laboratory Report UCRL-10925

73. J. I. Steinfeld (Ph. D. Thesis), Harvard University, Cambridge, Massachusetts, (1965).

74. E. Rabinowitch and W. C. Wood, Trans. Faraday Soc., 32, 540 (1936).

75. P. Sulzer and K. Wieland, Helv. Phys. Acta, 25, 653 (1952).

76. W. Klemperer, "private communication".

77. E. A. Ogryzlo and B. C. Sanctuary, J. Phys. Chem., 69, 4422 (1965).

78. D. B. Gibbs and E. A. Ogryzlo, Can. J. Chem., 43, 1905 (1965). The recombination of iodine atoms follows the same rate law; see D. L. Bunker and N. Davidson, J. Am. Chem. Soc., 80, 5085 (1958).

79. M. Alentsev, Doklady Akademiia Nauk SSSR, 62, 607 (1948).

80. H. Kopfermann and W. Tietze, Z. Physik, 56, 604 (1929).

FIGURE CAPTIONS

Fig. 1 Hatched area indicating the equivalent width of an absorption line. I^0 is the intensity of the continuum, and I_λ the intensity transmitted by the absorbing species.

Fig. 2 Coincidence circuit used by Branner, et al. to measure the lifetime of the state E_1.

Fig. 3 Block diagram of the short-lifetime apparatus.

Fig. 4 100 kc to 1 kc heterodyne circuit.

Fig. 5 360 kc to 1 kc heterodyne circuit.

Fig. 6 Frequency to voltage converter schematic. The DC output is fed to the beam power tubes of the motor speed-control power supply.

Fig. 7 Gain of the frequency-to-voltage converter circuit. Vertical broken lines indicate the linear operating region.

Fig. 8 Variation of beat frequency with the peak-to-peak voltage on the limiter grid (pin 2) of V4 in the frequency to voltage converter chassis. "A" is the usual operating region.

Fig. 9 Phase detector circuit. The reference signal inputs are $\pm e_1$, while the sample signal input is e_2.

Fig. 10 Reference channel one kilocycle amplifiers, phase shifter, and null detector.

Fig. 11 Sample channel one kilocycle amplifiers and phase shifter.

Fig. 12 Arrangement of apparatus used to measure the tracking and total phase shift of the reference and sample channel shifters. The auxiliary shifter is described by Berg (ref.30, p.12) and was modified to work at 1 kc.

Fig. 13 Voltage divider chain and cathode follower stage for the RCA 7265 multiplier phototube.

Fig. 14 Voltage divider chain and cathode follower stage for the Amperex 56 UVP multiplier phototube.

Fig. 15 Variation of relative phase across the sample channel light beam using the modulated Hg 5461Å line. The phase angle is measured from the starting point at 0 mm.

Fig. 16 Light modulating optics

L_1 Collimating lens

G Wire grating (100 strands/inch)

L_2 Lens for focusing grating on wheel

$s'/s = 1/5$

Fig. 17 (a) Measurement of scattered light from the sol. Wire screens or neutral density filters are placed in front of the photomultiplier to attenuate the scattered light.

(b) Measurement of a fluorescent signal at a temperature T from the resonance cell. In the I_2 lifetime measurements, Wratten filters were placed in front of the photomultiplier to block the incident wavelength(s).

Fig. 18 Lifetime of the mercury $^3P_1$ state vs fluorescence to scattered light intensity. Lifetime in the absence of entrapment $(I_f/I_s = 3 \text{ to } 10) = (1.10 \pm .05) \times 10^{-7}$ sec. Increase in lifetime with I_f/I_s is due to radiation entrapment.

Fig. 19 Stern-Volmer plot for continuum excitation peaked at 6040Å.

Fig. 20 Stern-Volmer plot for Na 5889, 5895Å excitation.

Fig. 21 Stern-Volmer plot for continuum excitation peaked at 5895Å.

Fig. 22 Stern-Volmer plot for continuum excitation peaked at 5592Å.

Fig. 23 Stern-Volmer plot for Hg 5461Å excitation.

Fig. 24 Stern-Volmer plot for continuum excitation peaked at 5461Å.

Fig. 25 Stern-Volmer plot for continuum excitation peaked at 5277Å.

Fig. 26 Stern-Volmer plot for continuum excitation peaked at 5168Å.

Fig. 27 Stern-Volmer plot for Cd 5086Å excitation.

Fig. 28 Stern-Volmer plot for continuum excitation peaked at 5087Å.

Fig. 29 Stern-Volmer plot for continuum excitation peaked at 5011Å.

Fig. 30 Variation of I_2-I_2 self-quenching cross section (top scale) and unquenched radiative lifetime (bottom scale) with vibrational level of the B state of I_2.

Fig. 31. Variation of absorption B-values with vibrational level.

Circles: Absorption coefficient $B_{a'}$, from all v" levels to the level a' = v', as given by Eq. (34).

Triangles: $B_{a'}$, values of Brown and Klemperer calculated from Eq. (33).

Solid Lines: Total band absorption measurements of Sulzer and Wieland (upper) and Rabinowitch and Wood (lower). Broken lines indicate the errors in the absorption measurements.

If the assumption $|R_e|$ = constant were valid, the circles would lie within the region enclosed by the broken lines.